1-1-2009

Central mass-to-light ratios and dark matter fractions in early-type galaxies

C. Tortora
Università di Napoli Federico II

N. R. Napolitano
INAF – Osservatorio Astronomico di Capodimonte

Aaron J. Romanowsky
San Jose State University, aaron.romanowsky@sjsu.edu

M. Capaccioli
Università di Napoli Federico II

G. Covone
Univ. Monte S. Angelo

Recommended Citation

C. Tortora, N. R. Napolitano, Aaron J. Romanowsky, M. Capaccioli, and G. Covone. "Central mass-to-light ratios and dark matter fractions in early-type galaxies" *Monthly Notices of the Royal Astronomical Society* (2009): 1132-1150. https://doi.org/10.1111/j.1365-2966.2009.14789.x

Mon. Not. R. Astron. Soc. **396,** 1132–1150 (2009) doi:10.1111/j.1365-2966.2009.14789.x

Central mass-to-light ratios and dark matter fractions in early-type galaxies

C. Tortora,[1,2,3★] N. R. Napolitano,[2] A. J. Romanowsky,[4] M. Capaccioli[3,5] and G. Covone[4,6]

[1]*INAF – Osservatorio Astrofisico di Catania, Via S. Sofia 78, I-95123 Catania, Italy*
[2]*INAF – Osservatorio Astronomico di Capodimonte, Salita Moiariello, 16, 80131 Napoli, Italy*
[3]*Dipartimento di Scienze Fisiche, Università di Napoli Federico II, Compl. Univ. Monte S. Angelo, 80126 Napoli, Italy*
[4]*UCO/Lick Observatory, University of California, Santa Cruz, CA 95064, USA*
[5]*INAF – VSTceN, Salita Moiariello 16, 80131 Napoli, Italy*
[6]*INFN – Sezione di Napoli, Univ. Monte S. Angelo, 80126 Napoli, Italy*

Accepted 2009 March 13. Received 2009 March 9; in original form 2008 December 24

ABSTRACT

Dynamical studies of local elliptical galaxies and the Fundamental Plane point to a strong dependence of the total mass-to-light ratio (M/L) on luminosity with a relation of the form $M/L \propto L^{\gamma}$. The 'tilt' γ may be caused by various factors, including stellar population properties (metallicity, age and star formation history), initial mass function, rotational support, luminosity profile non-homology and dark matter (DM) fraction. We evaluate the impact of all these factors using a large uniform data set of local early-type galaxies from Prugniel & Simien. We take particular care in estimating the stellar masses, using a general star formation history, and comparing different population synthesis models. We find that the stellar M/L contributes little to the tilt. We estimate the total M/L using simple Jeans dynamical models, and find that adopting accurate luminosity profiles is important but does not remove the need for an additional tilt component, which we ascribe to DM. We survey trends of the DM fraction within one effective radius, finding it to be roughly constant for galaxies fainter than $M_{\rm B} \sim -20.5$, and increasing with luminosity for the brighter galaxies; we detect no significant differences between S0s and fast- and slow-rotating ellipticals. We construct simplified cosmological mass models and find general consistency, where the DM transition point is caused by a change in the relation between luminosity and effective radius. A more refined model with varying galaxy star formation efficiency suggests a transition from total mass profiles (including DM) of faint galaxies distributed similarly to the light to near-isothermal profiles for the bright galaxies. These conclusions are sensitive to various systematic uncertainties which we investigate in detail, but are consistent with the results of dynamical studies at larger radii.

Key words: galaxies: elliptical and lenticular, cD – galaxies: evolution – galaxies: general – dark matter.

1 INTRODUCTION

Early-type galaxies (ETGs) are the most massive stellar systems in the Universe, containing much of the cosmic budget of visible and dark matter (DM). They include elliptical (E) and lenticular (S0) galaxies and form a nearly uniform class of objects: usually red, old and with only traces of cold gas and active star formation (SF). The striking regularities in their properties include strong correlations between size (e.g. the effective radius, $R_{\rm eff}$) and the surface brightness therein ($I_{\rm eff}$; Kormendy 1977), and between kinematics (the central velocity dispersion σ_0) and luminosity (L; Faber & Jackson 1976, hereafter FJ).

The two relations above merge into the so-called Fundamental Plane (FP; Djorgovski & Davis 1987; Dressler et al. 1987), i.e. a relation among the (logarithm of) σ_0, $R_{\rm eff}$ and $I_{\rm eff}$ of ETGs. The FP can be interpreted in terms of the virial theorem of relaxed systems, according to which $2T + U = 0$, where U is the potential energy and T is the kinetic energy. This can be rewritten in terms of observed quantities as approximately $L \propto \sigma^2 R_{\rm eff}$. However, the FP is found observationally to be $L \propto \sigma^{\eta} R_{\rm eff}^{\alpha}$ with $\alpha \neq 1$ and $\eta \neq 2$, i.e. a different orientation of the plane in the space of the logarithmic quantities with respect to the virial prediction. This *tilt* of the FP provides insight for the formation and structure of ETGs,

★E-mail: ctortora@na.astro.it

and can be interpreted as a variation of the total mass-to-light ratio (M/L) with L (Dressler et al. 1987) with the simplest parametrization as a power law, $M/L \propto L^{\gamma}$. The slope, γ, of this relation could be driven by one or more different factors: a variation in stellar M/L [due to metallicity or age gradient or change in initial mass function (IMF)], a variation in the DM content, non-homology, rotational support, etc. (see e.g. Busarello et al. 1997; D'Onofrio et al. 2006; Graves 2009). It is of considerable importance to disentangle these factors using high-quality data at low redshift, in order to use the FP as a guide to galaxy evolution in different environments and cosmic epochs (e.g. Kochanek et al. 2000; Bernardi et al. 2003; Reda, Forbes & Hau 2005; van Dokkum & van der Marel 2007).

Many studies over the years have attempted to decode the FP tilt (e.g. Renzini & Ciotti 1993; Hjorth & Madsen 1995; Pahre, Djorgovski & de Carvalho 1995, 1998a; Prugniel & Simien 1996, hereafter PS96; Graham & Colless 1997; Graham 1998; Pahre, de Carvalho & Djorgovski 1998b; Scodeggio et al. 1998; Mobasher et al. 1999; Bertin, Ciotti & Del Principe 2002; Nipoti, Londrillo & Ciotti 2002; Riciputi et al. 2005; di Serego Alighieri, Lanzoni & Jørgensen 2006; Bolton et al. 2007, 2008; Gargiulo et al. 2009). The emerging consensus is that stellar populations account for a minor fraction of the tilt (e.g. Trujillo, Burkert & Bell 2004, hereafter T+04; Cappellari et al. 2006, hereafter C+06; La Barbera et al. 2008; Proctor et al. 2008; Graves 2009; see however Jun & Im 2008), with the major contributor yet to be firmly identified – which would have ramifications for galaxy formation models (e.g. Capelato, de Carvalho & Carlberg 1995; Levine & Aguilar 1996; Kritsuk 1997; Bekki 1998; Ferreras & Silk 2000; Mathews & Brighenti 2000; Chiosi & Carraro 2002; Borriello, Salucci & Danese 2003; Dantas et al. 2003; González-García & van Albada 2003,Nipoti, Londrillo & Ciotti 2003; Evstigneeva et al. 2004; Aceves & Velázquez 2005; Boylan-Kolchin, Ma & Quataert 2005, 2006; Oñorbe et al. 2005, 2006; Dekel & Cox 2006; Robertson et al. 2006; Shankar et al. 2006; Almeida, Baugh & Lacey 2007; Hopkins, Cox & Hernquist 2008).

An additional complication is that the tilted FP may not be flat, with claims made for curvature (Zaritsky, Gonzalez & Zabludoff 2006; D'Onofrio et al. 2008; Hyde & Bernardi 2009b), and projections of the FP showing a bend at a characteristic magnitude of $M_{\rm B} \sim -20.5$ (see Section 2). This transition concords with more general findings of a discontinuity in ETG properties at a similar luminosity (e.g. Napolitano et al. 2008; Coccato et al. 2009).

Of particular interest is the FP contribution from the central DM content, since connecting luminous galaxies to their DM haloes is one of the key ingredients in modern recipes for galaxy assembly. The DM component of the FP tilt is currently a bone of contention, with findings alternatively of negligible impact (Gerhard et al. 2001, hereafter G+01; T+04), and of primary importance (Padmanabhan et al. 2004; C+06; Lintott, Ferreras & Lahav 2006). More generally, several lines of evidence point to a small but significant fraction of DM ($f_{\rm DM}$) inside 1 $R_{\rm eff}$ (e.g. G+01; Gavazzi et al. 2007; Weijmans et al. 2008), but the galaxies probed are typically very bright Es with $\sigma_0 > 200$ km s^{-1}. As data have become available on more 'ordinary' ETGs, there are suggestions that their DM properties vary strongly with luminosity, with perhaps even a dichotomy following the classic division of faint, discy, fast-rotating galaxies and bright, boxy, slow rotators (Capaccioli, Napolitano & Arnaboldi 2002; Romanowsky et al. 2003; Ferreras, Saha & Williams 2005; Napolitano et al. 2005, hereafter N+05; C+06; Douglas et al. 2007; van den Bosch et al. 2007; Ferreras et al. 2008; Covone et al. 2009; Napolitano et al. 2009a).

The purpose of this paper is to re-examine all the plausible factors that could contribute to the FP tilt. We will not be directly studying the FP, but rather will survey systematic trends in the central properties of ETGs which factor into the apparent M/L variation, γ. Our study springs from the classic data set of central photometry and kinematics of PS96, which is one of the largest such catalogues of local galaxies covering a wide range of luminosities. Our analysis consists of two parts, wherein we independently determine the stellar component of the M/L by stellar population models, and the total M/L by dynamical models. We take particular care in considering realistic SF histories, stellar population modelling systematics and dynamical contributions from DM.

We briefly describe the galaxy sample in Section 2 and analyse the stellar populations in Section 3. We determine the dynamical masses in Section 4 and infer the DM fractions in Section 5. Section 6 considers some implications for galaxy formation, and Section 7 draws conclusions and considers future prospects.

2 SAMPLE

Our data set of local ETGs is drawn from PS96.[1] This is currently one of the largest homogeneous samples of local ETGs available in the literature containing both photometry and kinematics of the galaxy central regions, and the only one including information on the peak rotation velocity ($V_{\rm max}$). As discussed in PS96, the colours (extinction- and K-corrected) are measured within 1 $R_{\rm eff}$, the central velocity dispersions σ_0 are recovered from long slit spectra[2] and $V_{\rm max}$ is defined as the quadratic sum of the maximum rotation on the major and minor axes. Since we are interested in fitting spectral energy distributions (SEDs), we select galaxies with at least two measured colours (most of the selected galaxies have four colours).[3] Selecting also for galaxies brighter than $M_{\rm B} = -16$, we recover ≈400 galaxies among which, following the PS96 classification, ≈55 per cent are bona fide Es (their subsample 1), ≈30 per cent are type S0 and Sa (their subsample 5), and the remaining ≈15 per cent are dusty objects, interacting galaxies, dwarf spheroidals, compact, dwarf, low-luminosity and peculiar ellipticals, etc. (subsamples 2, 3, 4 and 6). For the main purposes of this paper, we will use subsample 1 (hereafter 'Es') and 5 (hereafter 'S0s'), thus incorporating 335 galaxies, or ≈85 per cent of the PS96 sample.

In all the following, we use a cosmological model with ($\Omega_{\rm m}$, Ω_{Λ}, h) = (0.3, 0.7, 0.7), where $h = H_0/100\,{\rm km\,s^{-1}\,Mpc^{-1}}$ (Spergel et al. 2003), corresponding to a universe age of $t_{\rm univ} = 13.5$ Gyr.[4]

[1] Downloadable at http://vizier.cfa.harvard.edu/viz -bin/ VizieR?-source= J/A+A/309/749.

[2] The authors do not report detailed information about their measurement setup but, as extensively adopted in the literature analyses of this data set, we will interpret σ_0 as the luminosity-weighted velocity dispersion within a circular aperture of radius $R_{\rm eff}/8$.

[3] Apparent total magnitudes are on average slightly brighter than those in the RC3 catalogue (de Vaucouleurs et al. 1991) by -0.05 ± 0.1 mag, while the differences of $B - V$ and $U - B$ colours with those in RC3 are 0.00 ± 0.03 and -0.02 ± 0.03.

[4] The distance scale is critical for normalizing the luminosities and M/Ls. The distance moduli ($m - M$) from PS96, rescaled to $h = 0.7$, are on average lower than those reported in the RC3 catalogue (de Vaucouleurs et al. 1991) by $-0.11^{+0.26}_{-0.20}$ mag (uncertainties are 25 and 75th percentiles), while agreeing closely with estimates from Tonry et al. (2001) (shifted by -0.06 mag to correct to the Cepheid distance scale; Jensen et al. 2003) differing by $0.00^{+0.18}_{-0.16}$ mag.

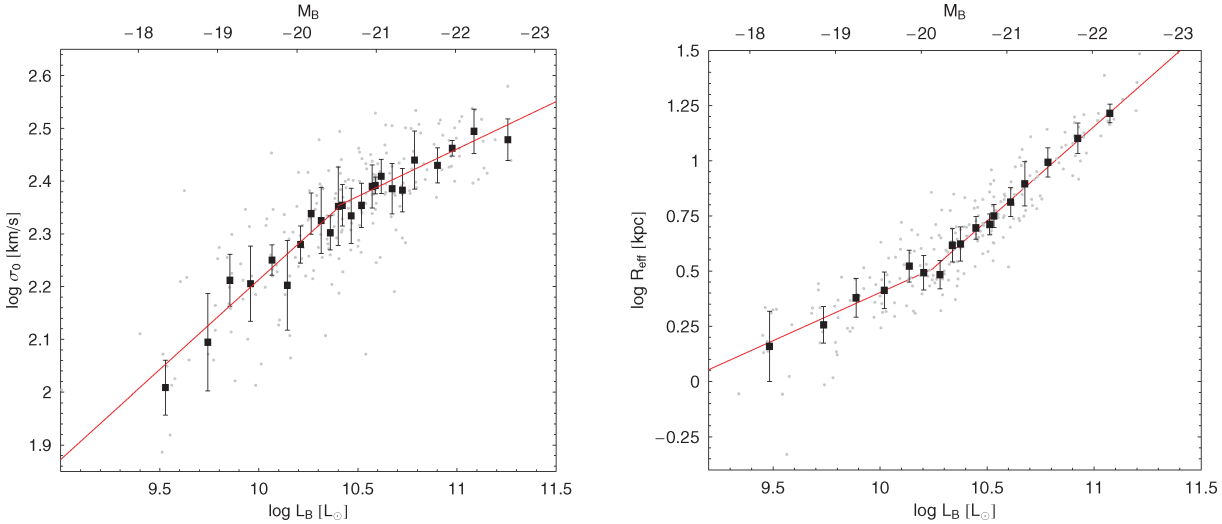

Figure 1. Correlations between photometric and kinematical properties of Es in our galaxy sample. The small points show individual galaxies, while the large points with error bars show binned averages. The solid lines show linear fits, carried out separately for the bright and faint subsamples (divided at $M_B \sim -20.5$, i.e. $\log L_B \sim 10.4\,L_\odot$). Left-hand panel: FJ relation. Right-hand panel: size–luminosity relation.

E galaxies populate a restricted region in the colour–magnitude diagram, the so-called 'red sequence', with a colour range of $B-V \sim$0.9–1. S0s span a wider range of colours (i.e. $B-V \sim$0.7−1) and are fainter than Es on average. The two subsamples follow similar FJ relations $L \propto \sigma_0^\eta$, including a characteristic magnitude ($M_B \sim -20.5$) where the relation clearly changes its slope (see left-hand panel of Fig. 1). For the E sample, $\eta = 2.9 \pm 0.5$ and 5.6 ± 1.2 for the faint and bright galaxies, respectively.

This FJ 'dichotomy' has been reported elsewhere (Matković & Guzmán 2005; Forbes et al. 2008), and seems related to systematic changes seen in other optical properties, e.g. the Kormendy relation (Capaccioli, Caon & D'Onofrio 1992; Nigoche-Netro, Ruelas-Mayorga & Franco-Balderas 2008), the Sérsic (1968) index (Caon, Capaccioli & D'Onofrio 1993; Prugniel & Simien 1997, hereafter PS97; Graham 1998; Graham & Guzmán 2003) and the size–magnitude relation (Shen et al. 2003; Bernardi et al. 2007; Desroches et al. 2007; Lauer et al. 2007; Hyde & Bernardi 2009a). The latter relation is illustrated for our sample Es in the right-hand panel of Fig. 1, where the faint and bright galaxies have fitted slopes of 0.85 ± 0.07 and 0.43 ± 0.11, respectively.

We will see that a characteristic luminosity scale is also found to characterize other correlations of ETG parameters.

3 STELLAR MASS-TO-LIGHT RATIO

One of the key aspects of our analysis is determining each sample galaxy's stellar M/L, $\Upsilon_\star$, which we do by fitting model SEDs to the observed galaxy colours. Although photometric modelling may seem less powerful than detailed spectroscopic fits, most spectroscopic samples are restricted to the very central regions of galaxies and may be very biased indicators of the stellar populations on scales of $\sim R_{\rm eff}$.

In Section 3.1, we describe the modelling procedure and present the recovered stellar population properties for the sample galaxies. We report the implications for the size–mass relation in Section 3.2, and for trends in $\Upsilon_\star$ in Section 3.3.

3.1 Stellar population modelling procedure

We create a set of synthetic stellar spectra using the prescription of Bruzual & Charlot (2003, hereafter BC03), which encompasses a wide range of initial metallicities and ages. A Salpeter (1955) or Chabrier (2001, 2002, 2003) IMF is assumed, with initial masses m in the range 0.1–100. The two IMFs do not influence the colours, but basically affect the $\Upsilon_\star$ estimates, which are ≈1.8 times larger with a Salpeter IMF than with a Chabrier IMF.

To generate a more general and realistic star formation history (SFH), we convolve the BC03 'single burst' models with an exponentially decaying SF rate with time t, $\propto e^{-t/\tau}$, where τ is a characteristic time-scale. The choice of BC03 is dictated mostly by its versatility and ability to span the stellar parameter space (metallicities and ages), but it is not the only prescription available on the market. We test for the presence of any modelling systematics mainly by checking different popular prescriptions, e.g. Bell & de Jong (2001, hereafter BdJ01) and Maraston (2005, hereafter M05) in Appendix A.

For each galaxy, we fit synthetic spectra to the observed colours ($U-B, B-V, V-R$ and $V-I$, after convolving the spectra with the appropriate filter bandpass functions), allowing us to estimate the age ($t_{\rm gal}$), metallicity (Z), τ, $\Upsilon_{*,B}$ and hence the stellar mass, $M_\star = \Upsilon_{*,B} \times L_B$ (hereafter we will always quote luminosity and M/L values in the B band, even if not specified). In detail, we build a set of synthetic colours with $Z \in (0.008, 0.02, 0.05)$,[5] $\tau \in$ (0.1–5) Gyr and $t_{\rm gal}$ up to $t_{\rm univ}$.[6] The fitting procedure consists of generating 100 Monte Carlo realizations of the observed galaxy colour sets assuming Gaussian errors of 0.05 mag per colour, and minimizing a χ^2 statistic between the modelled and observed colours for each realization. The overall best-fitting model parameters and

[5] Lower metallicities would have produced $t_{\rm gal}$ larger than the age of the universe in our assumed cosmology (∼13.5 Gyr).

[6] We allowed ∼10 per cent scatter around this value in order to account for some intrinsic uncertainty in the age estimates, and thus some of the estimated ages might be slightly larger than 13.5 Gyr.

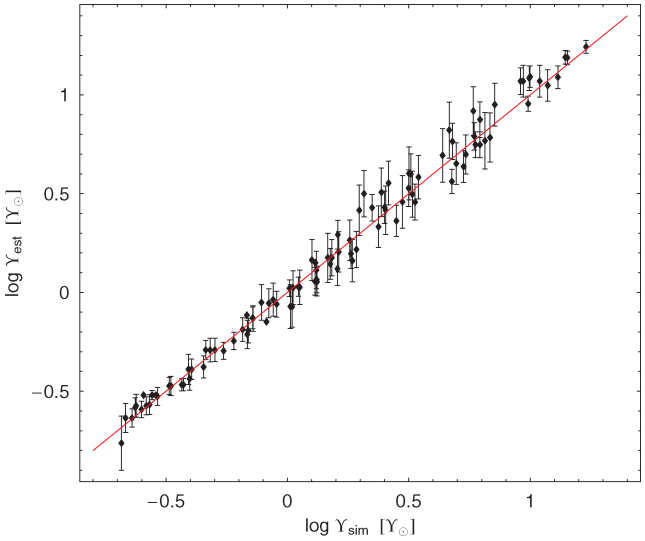

Figure 2. The Monte Carlo simulation of the stellar population fitting procedure, where the estimated stellar *M*/*L* values Υ_{est} are plotted against the intrinsic model values Υ_{sim}. The solid line is the one-to-one relation. The input value of $\Upsilon_\star$ is reproduced with no systematic bias, and the scatter of the recovered values is ∼10 per cent.

their uncertainties are defined as the median and scatter of these 100 best fits.[7]

Our synthetic modelling procedure is more general than the extensively used 'simple stellar population' (SSP) model where a galaxy is approximated as experiencing a single burst of SF (i.e. $\tau = 0$; Trager et al. 2000; M05; see also Appendix A). Instead we leave t_{gal}, τ and Z all as free parameters in order to better represent the wide variety of SFH expected both observationally and theoretically (see e.g. De Lucia et al. 2006; Noeske et al. 2007). The allowed ranges in the parameters will then be larger than in the more simplified SSP case because of the well-known degeneracies among them (Gavazzi et al. 2002; BC03).

To test the reliability of our modelling technique and the intrinsic parameter scatter, and to check for the presence of spuriously generated correlations, we run a suite of Monte Carlo simulations. We extract 100 simulated galaxy spectra from our BC03 SED libraries with random t_{gal}, Z and τ (i.e. with no correlation among these parameters), and apply our generalized fit procedure – comparing the recovered parameters with the input model values. We find that $\Upsilon_\star$ is recovered well, with a scatter of ∼10 per cent (see Fig. 2). Similar consistency is found for t_{gal}, Z and τ, which have on average larger scatter: ∼20, ∼30 and ∼30 per cent, respectively. We check for spurious correlations using a Spearman rank test (Press et al. 1992), finding that τ versus t_{gal} shows no correlation at the 95 per cent confidence level, but that t_{gal} and Z are weakly correlated, which is a common effect in stellar population analyses. However, this $t_{gal} - Z$ degeneracy does not affect the $\Upsilon_\star$ inference, which is our primary concern.

After fitting the real data for the complete sample of 335 galaxies, we show some relations between model parameters and other observed galaxy quantities in Fig. 3. From this figure, it is evident that the metallicity is generally solar or super-solar ($Z \geq 0.02$) and on average only weakly dependent on other properties such as luminosity – which is fortunate since the BC03 stellar libraries include only a few reference values for Z. More striking are the strong correlations involving t_{gal} and τ, such that the brighter, more massive galaxies formed their stars on average on shorter time-scales than the fainter, less massive galaxies, while the younger galaxies also had shorter SF time-scales (this does *not* mean that the brighter galaxies are younger, and if the S0s are included, the opposite is clearly true).

Similar findings on the SFHs of ETGs have been found in observational (e.g. Gavazzi et al. 2002; Thomas et al. 2005) and theoretical (e.g. De Lucia et al. 2006; Romeo et al. 2008) analyses. We will consider this subject in detail in a subsequent paper (Napolitano et al., in preparation), and for now summarize some basic parameters. The bright ETGs ($M_B \leq -20.5$) have a median $\tau \sim 0.5$ Gyr, while the faint ETGs have $\tau \sim 1$ Gyr. The Es have similar properties, while the S0s have on average more protracted SFHs ($\tau \sim$ 1–1.5 Gyr). The median $\Upsilon_\star$ for the ETGs is $6.9 \pm 2\,\Upsilon_\odot$ ($3.8 \pm 1.1\,\Upsilon_\odot$) for a Salpeter (Chabrier) IMF, where the quoted errors are the 1σ scatter. The S0s have only slightly smaller median $\Upsilon_\star$ than the Es: $6.2\,\Upsilon_\odot$ ($3.4\,\Upsilon_\odot$) and $7.1\,\Upsilon_\odot$ ($3.9\,\Upsilon_\odot$), respectively. However, the two samples differ more strongly in the *distribution* of $\Upsilon_\star$, where the Es have a fairly symmetric distribution about the mean, while the S0s have a pronounced tail to low $\Upsilon_\star$ such that the mean value of $5.8\,\Upsilon_\odot$ ($3.2\,\Upsilon_\odot$) differs from the median estimate.

3.2 Size–mass relations

An indirect way to test our derived $\Upsilon_\star$ values is to check how the implied scaling relation between size and stellar mass compares to previously established results. Expressing the size–*luminosity* relation as $R_{eff} \propto L^{\alpha_L}$, we find a slope for the Es of $\alpha_L = 0.70 \pm 0.06$, which is slightly steeper than some literature findings of 0.54–0.63 (Pahre et al. 1998a; Bernardi et al. 2003; Mamon & Łokas 2005). However, this slope is very sensitive to the range of luminosities fitted, since we see a difference between the 'faint' and 'bright' subsamples (see Section 2 and right-hand panel of Fig. 1).

For the size–mass relation $R_{eff} \propto M_\star^{\alpha_M}$, we obtain $\alpha_M = 0.58 \pm 0.05$ overall (Fig. 4), consistent with previous estimates for low-redshift galaxies of typically ∼0.6 (Bernardi et al. 2003; Shen et al. 2003; Mamon & Łokas 2005; N+05). This correlation also bends at a characteristic mass scale of $M_\star \sim 10^{11.1}\,M_\odot$, with $\alpha_M = 0.36 \pm 0.13$ and 0.73 ± 0.12 for the faint and bright galaxies, respectively (cf. Shen et al. 2003). We find the S0s to have on average smaller R_{eff} than Es of the same mass, and similar α_M at high masses, but flattening to be ∼0 at low masses.

3.3 Luminosity dependence of $\Upsilon_\star$

The central regions of ETGs are probably dominated by the stellar mass, so it is of critical importance to ascertain the fraction of the FP tilt that is connected to the stellar population properties. We focus on the relation $\Upsilon_* \propto L_B^{\gamma_*}$ in the log–log space, fitting to weighted medians of binned data values, with results that are stable to changes in the binning (Fig. 5). For the overall ETG sample, we find a slope of $\gamma_\star = 0.06 \pm 0.01$; the Es have $\gamma_\star = 0.02 \pm 0.01$, and S0s have $\gamma_\star = 0.17 \pm 0.03$, although this steeper slope is driven by the very faintest galaxies ($M_B > -19$).

Before taking these results at face value, we investigate possible dependencies on modelling systematics. Changing the IMF from Salpeter to Chabrier does not affect $\gamma_\star$, but only the overall normalization of $\Upsilon_\star$. Adopting a simplified model with t_{gal} as the only

[7] Typical 1 σ uncertainties on the estimated $\Upsilon_\star$ are ∼10–20 per cent. In general, in this paper, we will fit *medians* rather than *means* in order to be more robust to outliers.

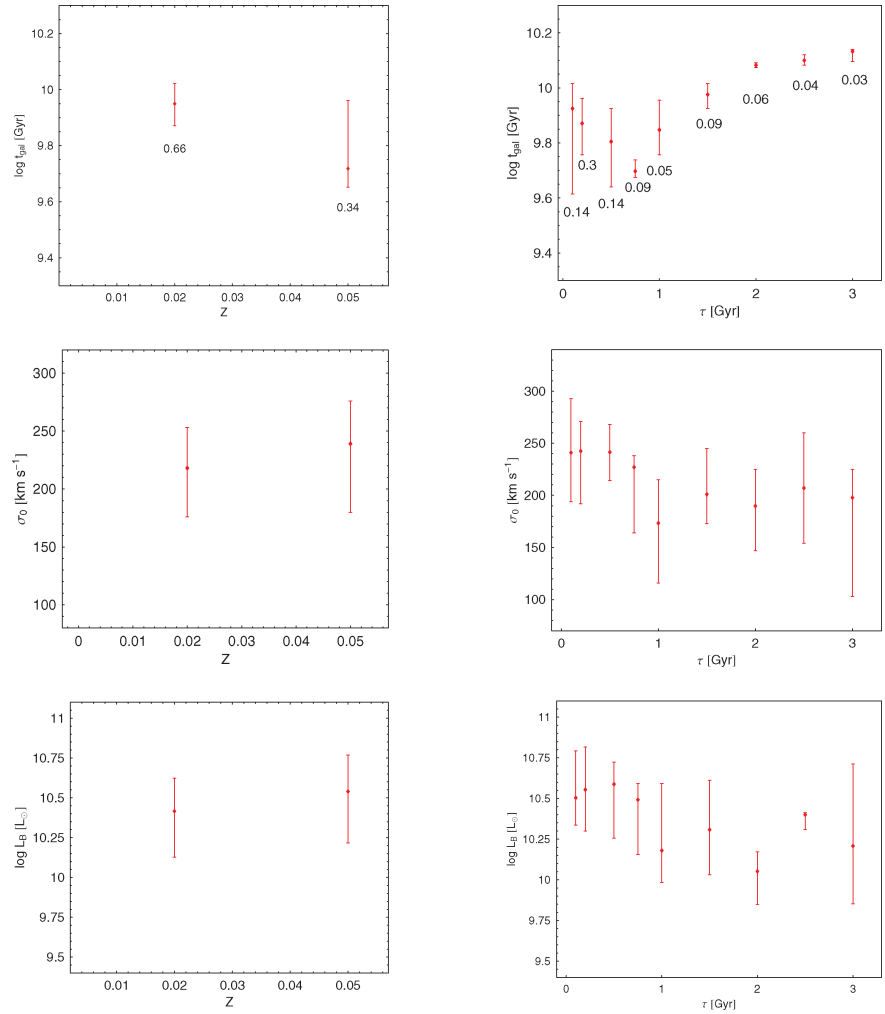

Figure 3. Stellar population properties of E sample galaxies: metallicity Z, SF time-scale τ, stellar age $t_{\rm gal}$ and luminosity $L_{\rm B}$. In each panel, the data are binned in intervals, with the median and ±25 per cent scatter shown. The fraction of galaxies in each bin is reported in the first two panels. For S0s, the trends with metallicity are identical to the Es, while the ones with τ are weaker.

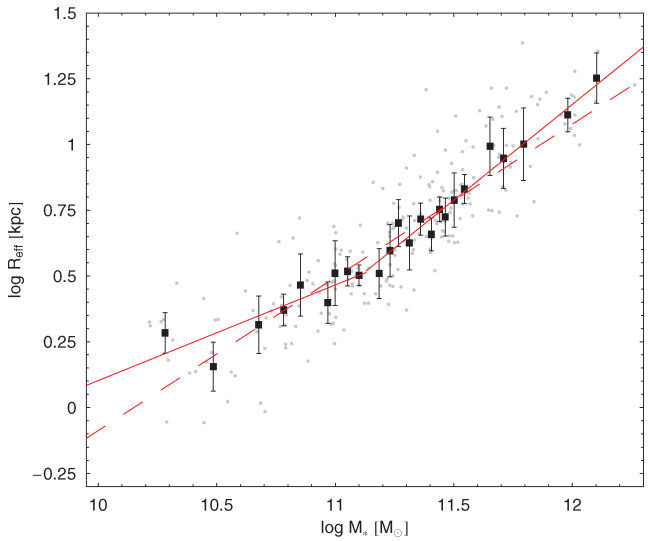

Figure 4. Correlation between effective radius and stellar mass in E galaxies. The symbols are as in Fig. 1. The dashed line is the best-fitting relation over the full range of the data, while the solid line is the best fit to the two mass regimes.

free parameter, with $\tau \sim 0.75$ Gyr and $Z \sim Z_\odot$ fixed to the median values for the whole sample (see Section 3.1), $\Upsilon_\star$ steepens for the faint galaxies and flattens for the bright ones, with an overall result of $\gamma_\star \sim 0.16$ (Appendix A). An even more simplified SSP model with $\tau = 0$ yields about the same $\gamma_\star \sim 0.18$. Thus, we see that allowing for the variations of SF time-scales (and metallicity) within the sample is critical for accurately deriving the $\Upsilon_\star$ trends with luminosity. An additional complication, only partially addressed by our model's protracted exponential SFH, is multiple bursts of SF in a single galaxy which, if corrected for, would probably flatten the slope even further (cf. section 4.7 of C+06).

We next consider alternative stellar population basis models. As detailed in Appendix A, adopting the BdJ01 or M05 models with the same assumptions would imply shallower and steeper $\Upsilon_\star$ slopes, respectively. This turns out to be the dominant source of uncertainty in the analysis, although the uncertainty is largest for the faintest galaxies ($M_{\rm B} \gtrsim -20.5$), and $\Upsilon_\star$ estimates more stable for the brighter galaxies.[8]

[8] Including all the systematics, the final slope becomes $\gamma_\star = 0.06 \pm 0.01^{+0.12}_{-0.04}$.

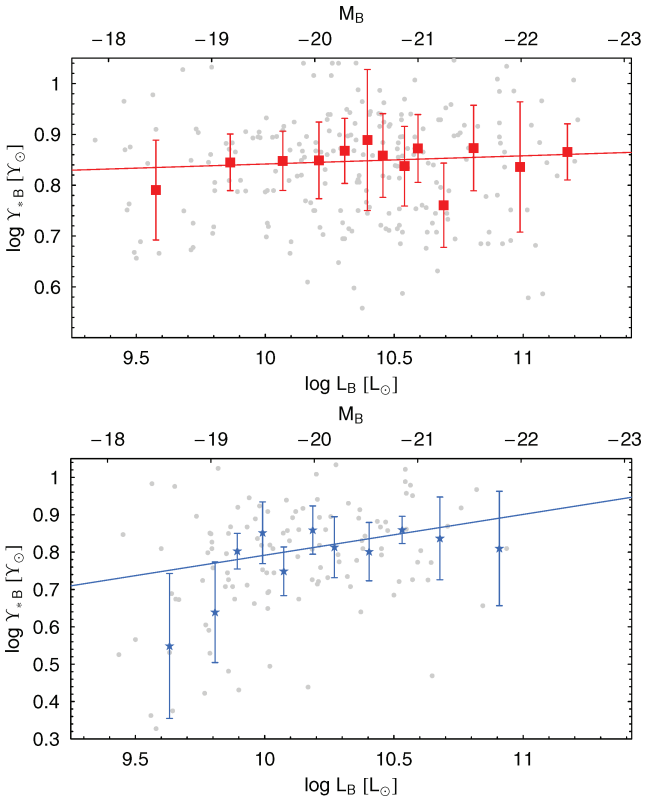

Figure 5. Stellar M/L as a function of B-band luminosity, for Es (top panel) and S0s (bottom panel). Grey points represent individual galaxies, while points with error bars are binned median values and scatter. Solid lines are the best-fitting linear relations in the log–log space. A Salpeter IMF is assumed.

How do our results compare to previous work? As mentioned in Section 1, most recent studies agree that $\gamma_\star$ is a relatively small contributor to the total γ of the FP. For example, PS96 inferred from the same data set that $\gamma_\star \sim 0.1$, and T+04 found using very different data and techniques that $\gamma_\star = 0.07 \pm 0.01$ in the B band.[9] This general consistency is encouraging, but it should be kept in mind that, as just discussed, there remain significant uncertainties in the modelling.

The foregoing conclusions are based upon a universal IMF, but there are suspicions that the IMF may vary with time or environment (e.g. Davé 2008; van Dokkum 2008). Renzini & Ciotti (1993) pointed out that a variation in the IMF with luminosity could easily account for the FP tilt. Here, we illustrate this point again with a simple toy model, wherein the faint galaxies have a Chabrier IMF and the bright ones a Salpeter IMF (a more realistic scenario would have the IMF changing smoothly with luminosity). The implied $\Upsilon_\star$ slope would be $\gamma_\star \sim 0.3$ (Fig. 6), which as we will see would be enough to explain the FP tilt with no further ingredients (e.g. no DM).

[9] For the modelling, PS96 used fitting relations linking single colours and line-strength index Mg_2 to the magnitude. T+04 applied the PEGASE prescription (Fioc & Rocca-Volmerage 1997) to the Sloan Digital Sky Survey (SDSS) Early Data Release. T+04 also found $\gamma_\star = 0.02 \pm 0.01$ in the K band using Two-Micron All-Sky Survey data (Bell et al. 2003), but one would expect $\gamma_\star$ to depend on bandpass because of the changing contributions from the mix of stellar populations.

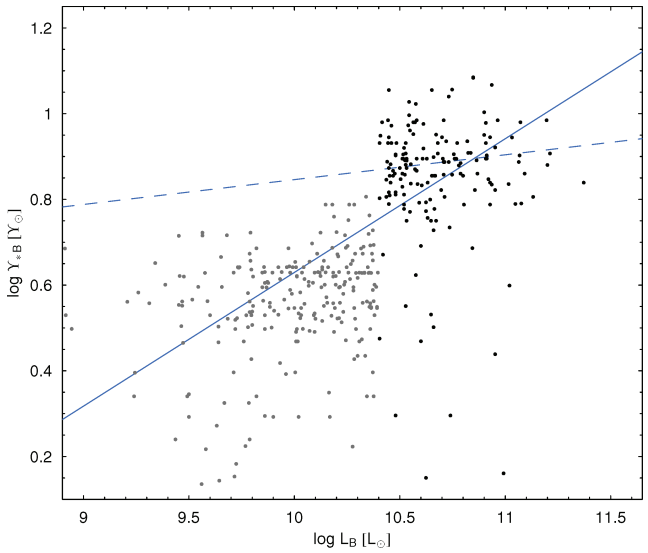

Figure 6. Stellar M/L for ETGs as a function of B-band luminosity, assuming an arbitrary change in the IMF at intermediate luminosity $\log(L/L_\odot) = 10.4$. The faint galaxies (grey points) have a Chabrier IMF and the bright galaxies (black points) a Salpeter IMF. The blue solid line is the best fit, while the dashed one is the relation with a constant Salpeter IMF.

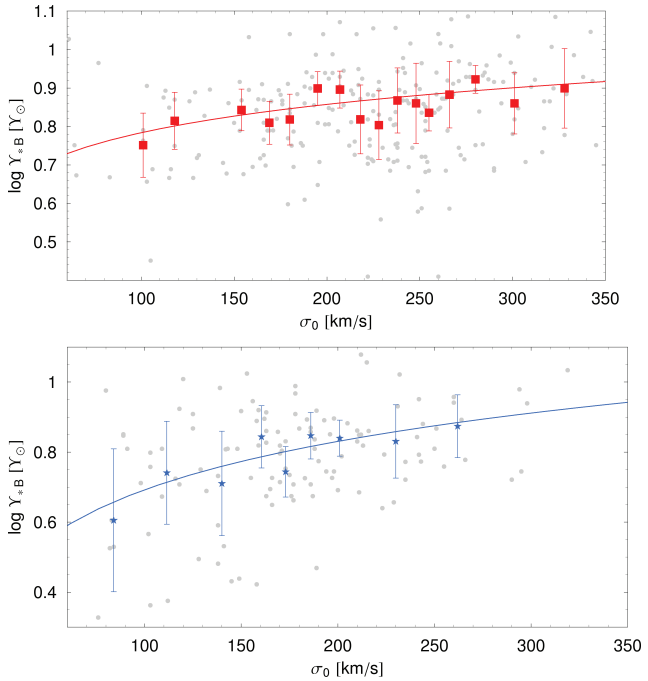

Figure 7. Stellar M/L ratio as a function of velocity dispersion σ_0, using Salpeter IMF for Es (top panel) and S0s (bottom panel) (see Fig. 5 for colour code and other details).

We lastly examine the correlation of $\Upsilon_\star$ with velocity dispersion: $\Upsilon_* \propto \sigma_0^{\gamma_\sigma}$. The fitted slope is $\gamma_\sigma \sim 0.2$–0.4 for both Es and S0s (Fig. 7). The steepness of this trend relative to $\gamma_\star$ suggests that the stellar populations of galaxies are more strongly linked to their dynamical masses than to their luminosities. This issue will be considered in more detail in the following sections, and as part of a separate analysis in Napolitano et al. (in preparation).

4 DYNAMICAL MASS

Besides $\Upsilon_\star$, the other fundamental quantity we want to determine is the total dynamical M/L, $\Upsilon_{\rm dyn}$. The usual way the dynamical mass is calculated in FP studies is with the virial relation

$$M = \frac{K\sigma_0^2 r}{G}, \tag{1}$$

where G is the gravitational constant and K is a pressure correction coefficient (or virial coefficient; e.g. Eke et al. 2004; Padmanabhan et al. 2004; C+06). The K factor subsumes a host of issues such as the aperture wherein σ_0 is measured, and variations or 'non-homologies' in the viewing angles, orbital structures, luminosity profile, DM distribution, etc.

Rather than adopting some approximate value or function for K, we will here directly model the non-homologies as much as possible for every individual galaxy in the sample, using the Jeans equations to estimate $\Upsilon_{\rm dyn}$ within 1 $R_{\rm eff}$. We outline the modelling methods in Section 4.1, present results based on luminosity profile homology in Section 4.2 and on more general profiles in Section 4.3.

4.1 Dynamical methods

The basic approach of our dynamical models is to take the observed luminosity profile for each galaxy, along with a parametrized mass model, and solve for the projected velocity dispersion σ_0 within a central aperture. The mass model parameters are then optimized to match the observed value for σ_0.

In detail, the steps are as follows.

(i) We parametrize the luminosity profile $j_\star(r)$ by either a (de-projected) de Vaucouleurs (1948) profile or a more general Sérsic (1968) model (Caon et al. 1993) – which fully takes into account any non-homologies in the stellar density distributions. The functional form for $j_\star(r)$ is specified in appendix B of PS97.

(ii) We adopt a simplified form for the total cumulative dynamical mass profile $M(r)$ which is either a constant-M/L profile $M(r) = \Upsilon_0\, L(r)$ (including the cases where DM is missing or has a cored distribution; see Burkert 1995; Napolitano et al. 2009a) or a singular isothermal sphere (SIS), where $M(r) \propto \sigma^2_{\rm SIS} r$. The latter choice is motivated by evidence from strong gravitational lensing for near-SIS profiles in the central regions of ETGs (e.g. Kochanek 1991; Koopmans et al. 2006). These two alternatives bracket the plausible range of mass profiles.

(iii) We solve the Jeans equation:

$$\frac{{\rm d}\left(j_* \sigma_r^2\right)}{{\rm d}r} + 2\,\frac{\beta(r)}{r}\, j_* \sigma_r^2 = -j_*(r)\,\frac{GM(r)}{r^2}, \tag{2}$$

where $\beta = 1 - \sigma_t^2/\sigma_r^2$ is the anisotropy. This model assumes spherical symmetry and no rotation (cf. Mamon & Łokas 2005). For simplicity, we also assume isotropy ($\beta = 0$), in which case the Jeans equation (2) can be transformed to

$$\sigma_r^2(r) = \frac{1}{j_*(r)} \int_r^\infty j_* \frac{GM}{s^2}\,{\rm d}s. \tag{3}$$

(iv) We project equation (3) to obtain the line-of-sight velocity dispersion:

$$\sigma^2_{\rm los}(R) = \frac{2}{I(R)} \int_R^\infty \frac{j_* \sigma_r^2\, r\,{\rm d}r}{\sqrt{r^2 - R^2}}, \tag{4}$$

where

$$I(R) = 2\int_R^\infty \frac{j_*\, r}{\sqrt{r^2 - R^2}}{\rm d}r \tag{5}$$

is the projected density profile.

(v) We integrate $\sigma_{\rm los}$ within a fixed aperture $R_{\rm eff}/8$ to obtain the aperture velocity dispersion, $\sigma_{\rm Ap}$ using the equation

$$\sigma^2_{\rm Ap}(R_{\rm eff}/8) = \frac{1}{L(R_{\rm eff}/8)} \int_0^{R_{\rm eff}/8} 2\pi\, SI(S)\, \sigma^2_{\rm los}(S)\,{\rm d}S, \tag{6}$$

where $L(R) = \int_0^R 2\pi SI(S)\,{\rm d}S$ is the luminosity within the projected radius R.[10]

(vi) We fit the model $\sigma_{\rm Ap}$ to the observed σ_0 and iterate the preceding steps, varying the free parameters in equation (3) (i.e. $\sigma_{\rm SIS}$ or Υ_0). The resulting best-fitting mass profile then provides the total spherical mass-to-light ratio within an effective radius $\Upsilon_{\rm dyn}(R_{\rm eff})$ (which is coincident with Υ_0 in the case of the constant-M/L model).

This procedure does not take into account certain factors that could, in principle, alter the final mass estimates. First, the mass model does not include a central black hole, but we calculate the effect to be negligible.[11] More importantly, real galaxies are neither spherical nor isotropic in general. We will check the impact of these simplifications later, but here begin with a first-order correction to the isotropic results.

Detailed dynamical models of nearby galaxies have shown that their central stellar parts are close to isotropic *after subtracting the rotational component* (e.g. G+01; C+06; Cappellari et al. 2007). The observed $\sigma_{\rm Ap}$ does incorporate both the projected rotation and dispersion components of the specific kinetic energy ($\sigma^2_{\rm Ap} = v^2_{\rm rms} = v^2 + \sigma^2$), and the Jeans equations could in principle be reformulated along these lines. However, for many galaxies the rotation is so dominant that it is preferable to include it as an additional, separate term, which would require additional assumptions about the rotation field of each galaxy, and would best entail a non-spherical treatment anyway – all of which is beyond the scope of this paper.

Here, we adopt a heuristic correction to the *observed* dispersion in order to approximately account for rotational effects. Following PS94, we parametrize the corrected $\sigma'_{\rm Ap}$ by $\sigma'_{\rm Ap} = \sigma_{\rm Ap}\,\delta_{\rm rot}$. To estimate $\delta_{\rm rot}$, we have performed Monte Carlo simulations as in Napolitano et al. (2001), beginning with a suite of analytical spherical stellar + DM models as described in N+05[12]. For each model with a fixed gravitational potential, we assume isotropy and an additional rotational component that increases with radius, then solve the Jeans equations and project to $\sigma_{\rm Ap}$. Finally, we examine the factor $\delta_{\rm rot}$ that relates the rotating and non-rotating 'measurements' $\sigma_{\rm Ap}$, finding this simple approximation:

$$\delta_{\rm rot} \approx 1 + 0.05\frac{V_{\rm max}}{\sigma_0}, \tag{7}$$

[10] We check that using an aperture of $R_{\rm eff}/10$ would leave the results almost unchanged. Following T+04, we have also checked that alternatively using fixed apertures of 1.6 and 2.2 arcsec, the median $\Upsilon_{\rm dyn}$ values are overestimated by 3^{+3}_{-2} and 1^{+3}_{-1} per cent, well within the typical uncertainty on each estimate and on the sample's global scatter.

[11] We added an estimated black hole mass $M_{\rm BH}$ in the Jeans equations, using $M_{\rm BH}$ predicted by the correlation $\sigma_0 - M_{\rm BH}$ in Ferrarese & Merritt (2000). The result was to decrease $\Upsilon_{\rm dyn}$ by 2 ± 1 per cent.

[12] The multicomponent model, in their Section 3, includes a Hernquist (1990) stellar distribution and an NFW (Navarro, Frenk & White 1996, 1997) spherical DM halo.

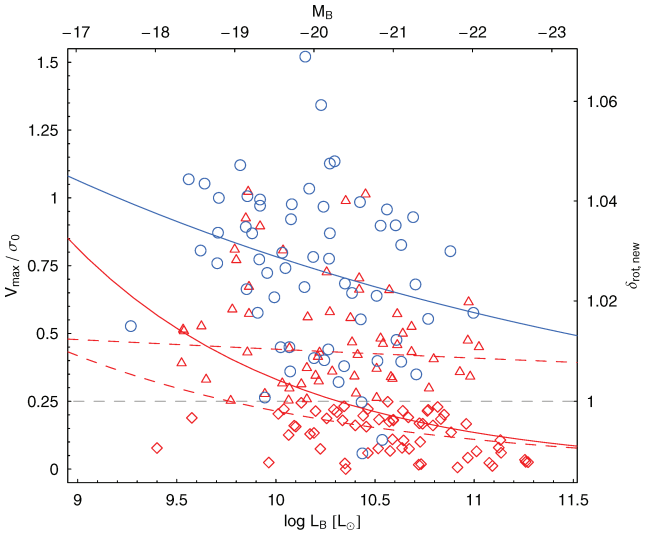

Figure 8. Ratio between rotation and dispersion of ETG sample, as a function of luminosity. Red diamonds, red triangles and blue circles are, respectively, slow-rotator Es, fast-rotator Es and S0s. The solid red and blue curves are functional fits to the binned data, for Es and S0s, respectively, while the red dashed ones are for slow- and fast-rotator Es. Finally, the dashed grey line sets the boundary between slow and fast rotators.

which is calculated for an aperture of 1 $R_{\rm eff}$ and turns out to be valid for a large range of galaxy masses.[13] We therefore apply this correction to the observed $\sigma_{\rm Ap}$ before matching to the models in step (vi) above. The correction increases the inferred $\Upsilon_{\rm dyn}$ values since rotation at $\sim R_{\rm eff}$ coupled with the $\beta = 0$ assumption depresses the central σ_r for a given mass profile: a rotational component must be subtracted from the right-hand side of equation (3).

The trend with luminosity for the rotation correction in our galaxy sample is shown in Fig. 8, implying $\Upsilon_{\rm dyn}$ corrections of $\sim$1 per cent for the brightest Es, and $\sim$6 per cent for the faintest S0s (as is well known, rotation is a stronger factor on average among fainter ETGs). When plotting results for all galaxies in the sample we use the median $(V_{\rm max}/\sigma_0) - L_{\rm B}$ trend to estimate their $\delta_{\rm rot}$. Where possible, we also classify the Es as fast or slow rotators, using $V_{\rm max}/\sigma_0 = 0.25$ as the demarcation – a simple scheme that matches the more robust conclusions of C+06 in more than 90 per cent of the overlapping cases.

4.2 Results from homologous luminosity profiles

We can now derive $\Upsilon_{\rm dyn}$, starting with the simplest case where we assume no rotation, and a homologous model for the luminosity distribution $j_\star(r)$: an $R^{1/4}$ profile which is completely determined by the known $L_{\rm B}$ and $R_{\rm eff}$ for every galaxy. For the mass profile, we initially assume the SIS model. Fitting the σ_0 data, we show the mass–luminosity results in Fig. 9 (left-hand panel). Binning the data, we fit the median relation $\Upsilon_{\rm dyn} \propto L_{\rm B}^{\gamma_{\rm dyn}}$ and find $\gamma_{\rm dyn} = 0.21 \pm 0.01$. This is identical to the one for the E subsample alone, $\gamma_{\rm dyn} = 0.21 \pm 0.01$ (see Table 1). The S0s show a larger scatter and have a global slope of $\gamma_{\rm dyn} = 0.18 \pm 0.03$, which steepens for faint galaxies ($M_{\rm B} > -20.5$, $\gamma_{\rm dyn} \sim 0.3$) and appears to flatten or even *decrease* at higher luminosities ($\gamma_{\rm dyn} \leq 0$). These slope results are scarcely changed by including the rotational correction (see Table 1), although the *normalization* of $\Upsilon_{\rm dyn}$ is increased for the S0s (see Fig. 9, right-hand panel), an issue to which we will return in Section 5.

Previous dynamical studies of ETGs using $j_\star$ homology have found a variety of tilt slopes, ranging from $\gamma_{\rm dyn} \sim 0.1$ to $\sim$0.3 (e.g. Jorgensen, Franx & Kjaergaard 1993; Bernardi et al. 2003; Padmanabhan et al. 2004; T+04). The average of the literature B-band values in Table 1 of PS96 yields $\gamma_{\rm dyn} = 0.25 \pm 0.05$, consistent with our result.

Now considering the other extreme assumption for the mass model, constant M/L, the extrapolation to $R_{\rm eff}$ after fitting to σ_0 changes the $\Upsilon_{\rm dyn}$ normalization, corresponding to $K = 2.05$ at $R_{\rm eff}$ in equation (1) for SIS, and $K = 1.93$ for constant M/L . The *slope* of the $\Upsilon_{\rm dyn} - L_{\rm B}$ relation is on the other hand unchanged (see Table 1). The K difference does raise the interesting possibility of mass profile non-homology, e.g. a systematic change with luminosity. As with the IMF toy model in Section 3.3, we can consider an arbitrary case where the faintest galaxies have constant-M/L profiles, and the brightest ones have SIS. This would increase $\Upsilon_{\rm dyn}$ by $\sim$0.02, i.e. mass non-homology does not appear to be a significant contributor to the FP tilt, assuming $j_\star$ homology.

4.3 Results from generalized luminosity profiles

We next relax the $j_\star$ homology assumption, allowing for more realistic luminosity profiles based on the Sérsic law, with surface brightness profiles expressed as

$$\mu(R) \propto C - (R/R_{\rm eff})^{1/n}, \qquad (8)$$

where C is a constant and n is an index of profile curvature which correlates with luminosity, such that the brighter galaxies have higher n (less curved profiles; e.g. Caon et al. 1993; Graham 1998; Graham & Guzmán 2003; Mamon & Łokas 2005; Kormendy et al. 2009). As illustrated by equation (2), for a given dispersion profile, changing the shape of $j_\star(r)$ will affect the inferred mass. Thus it is important to explore the impact of $j_\star$ non-homology on $\Upsilon_{\rm dyn}$, which may be expressed as a trend with luminosity $K = K(n|L_{\rm B})$. This is all a fancy way to say that *accurate dynamical results require accurate luminosity profile models.*

The $n-L_{\rm B}$ correlation has been investigated for our galaxy sample by PS97. From the overall ETG sample in their fig. 5, we define a simple relation where $n \sim L_{\rm B}^{0.2}$ for $M_{\rm B} > -20$ and $n = 4$ for all the brighter galaxies.[14] This relation also applies for the E subsample, and we assume that it does for the S0s as well.

We now use the $n-L_{\rm B}$ relation to construct the $j_\star(r)$ Sérsic profile for each galaxy as needed for the dynamical modelling (Section 4.1). Since we have examined the effects of rotation in Section 4.2, we will here skip over the simplified case of no rotation. The resulting $\Upsilon_{\rm dyn}$ values for both SIS and constant-M/L cases are summarized

[13] This correction is much smaller than that found by PS94 because these authors did not take into account the variations of rotation with radius nor of the measurements made within an aperture rather than along the major axis.

[14] PS97 noted that at least one other study found higher values of n for the brightest galaxies, but commented that those results were more sensitive to the outer profiles than to the central regions of relevance here. Similar concerns might apply to the recent smaller galaxy sample of Kormendy et al. (2009), but it is beyond the scope of our paper to re-investigate n dependencies in detail. If n were systematically higher for the brighter galaxies, then these systems' $\Upsilon_{\rm dyn}$ results would be *lower* (cf. next footnote). Note also that the $R_{\rm eff}$ values that we use were obtained by $R^{1/4}$ fitting in PS96 rather than the self-consistent Sérsic values, which could in principle affect the results for the fainter galaxies.

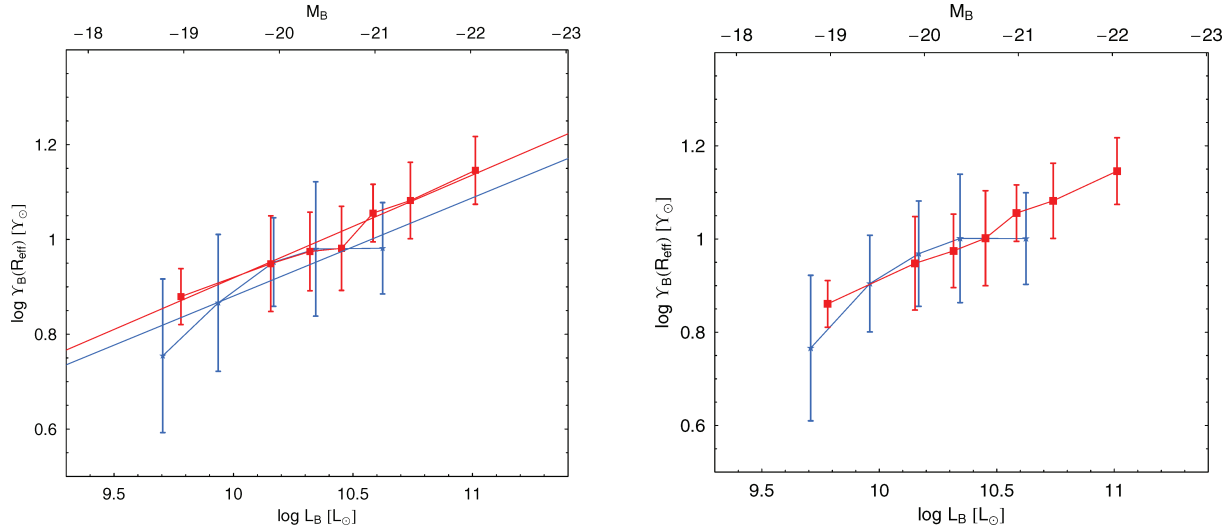

Figure 9. Dynamical M/L in B band within $R_{\rm eff}$ as a function of luminosity assuming $j_\star$ homology and an SIS total mass profile. Red squares and blue stars denote E and S0 galaxies, respectively. Points with error bars are the median values and ±25 per cent scatter for the galaxies in luminosity bins. Left-hand panel: no rotation assumed. Linear best fits to the binned data are overplotted as straight lines. Right-hand panel: correction made for rotational support.

Table 1. Slope of $M/L - L_{\rm B}$ relation for Es and S0s and different dynamical models (the Sérsic profiles assume the $n - L_{\rm B}$ relation discussed in the text). The first five rows are the slope for the total (dynamical) mass, and the last row due to stars only, as derived with our stellar population model (Section 3).

Model	$\gamma_{\rm E}$	$\gamma_{\rm S0}$	$\gamma_{\rm tot}$
$R^{1/4}$+SIS	0.21 ± 0.01	0.18 ± 0.03	0.21 ± 0.01
$R^{1/4}$+SIS+rot	0.20 ± 0.01	0.18 ± 0.03	0.20 ± 0.01
$R^{1/4}$+const M/L+rot	0.20 ± 0.01	0.18 ± 0.03	0.20 ± 0.01
Sérsic+SIS+rot	0.21 ± 0.01	0.20 ± 0.03	0.21 ± 0.01
Sérsic+const-M/L+rot	0.10 ± 0.01	0.10 ± 0.03	0.13 ± 0.02
Stars	0.02 ± 0.01	0.17 ± 0.03^a	0.06 ± 0.01

[a]The faintest S0s have a steeper slope than the brighter ones (see Fig. 5). Uncertainties on slopes are the 1σ scatter computed by a bootstrap method.

in Table 1 and Fig. 10. For the SIS case, relaxing the $j_\star$ homology slightly changes the slope $\gamma_{\rm dyn}$. However, in the constant-M/L case, both the luminosity *and* mass profiles are affected, and significant differences arise. The masses are increased for the fainter galaxies[15], causing the $\Upsilon_{\rm dyn}$ slope to become shallower overall ($\gamma_{\rm dyn} = 0.13 \pm 0.02$), and even constant at lower luminosities ($\gamma_{\rm dyn} = 0.05 \pm 0.04$ and 0.23 ± 0.02 for the faint and bright Es, respectively). The Es and S0s are again not notably different in their region of luminosity overlap. In Appendix B, we investigate systematic uncertainties in these results, whose impact we will consider in the next section.

Now reviewing the results of this and the previous sections, with the $j_\star$ homology assumption, the steep $\Upsilon_{\rm dyn}$ slope relative to $\Upsilon_\star$ ($\gamma_{\rm dyn} = 0.20$ versus $\gamma_\star = 0.06$) would imply that ∼75 per cent of the FP tilt is related to DM content or some other factor. Including the (realistic) $j_\star$ non-homologies changes the picture somewhat: if all galaxies have SIS mass profiles, the previous conclusion is unchanged. If they have steeper mass profiles, then the dynamical contribution to the tilt decreases, and for the fainter galaxies may even disappear.

Thus our results suggest overall that DM contributes to the tilt for the brightest galaxies, while the contribution for the fainter galaxies is unclear but probably less. This conclusion differs from that of T+04, who found using similar Sérsic models and *assuming constant M/L*, no need for a correlation between DM fraction and luminosity.

Their galaxy sample is fainter and much smaller, so their results are actually consistent with ours in general. The exception is for the brightest galaxies, where the higher n-values of T+04 lead to less tilt than we find. In any case, it should be noted that reproducing the FP tilt without DM variation is not a unique solution, and as we have shown, DM could still be a primary driver of the tilt.

5 DARK MATTER FRACTIONS

Having analysed the trends for stellar and total mass in our galaxy sample, we now examine the implications for DM content. We define the DM fraction within the three-dimensional radius $r = 1$ $R_{\rm eff}$ by

$$f_{\rm DM} = \frac{M_{\rm tot} - M_*}{M_{\rm tot}} = 1 - \frac{\Upsilon_*}{\Upsilon_{\rm dyn}}, \quad (9)$$

where for physically meaningful results we should have $\Upsilon_\star \leq \Upsilon_{\rm dyn}$ and thus $f_{\rm DM} \geq 0$. Strictly speaking, our derived $\Upsilon_\star$ should be *deprojected* before computing $f_{\rm DM}$, but we do not have the information necessary to do so. Given the negative colour gradients in ETGs, we expect the deprojected $\Upsilon_\star$ to be somewhat higher than in projection, and thus the true $f_{\rm DM}$ to be somewhat lower. For this reason and especially because of the large IMF uncertainty, *the absolute values for $f_{\rm DM}$ are not definitive, but instead the relative variations are more robust and are the focus of our study.*

We now consider the $f_{\rm DM}$ trends found for our galaxy sample, taking as a default the $\Upsilon_\star$ estimates from the generalized

[15] This is because lower n for the fainter galaxies implies shallower central profiles of both luminosity and mass density, and therefore lower central velocity dispersions at a fixed mass, finally requiring higher model masses to match the observations. This effect might be somewhat reversed by the central cusps of light generally found in faint Es to be superimposed on their overall Sérsic profiles, in many cases on spatial scales comparable to the σ_0 measurement (e.g. Kormendy et al. 2009), but it is beyond the scope of this paper to consider this possibility in detail.

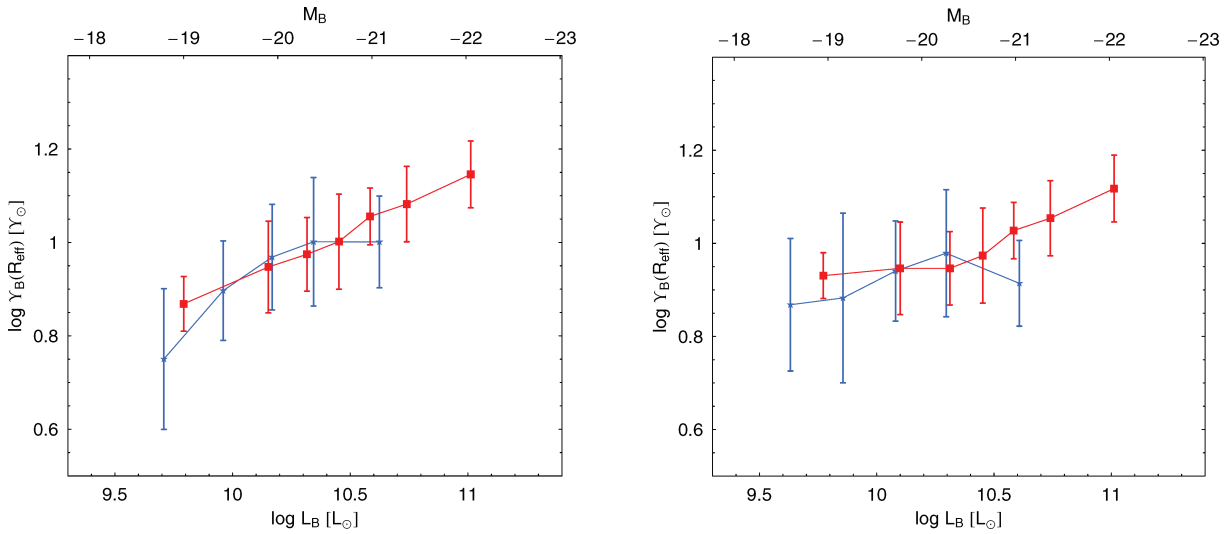

Figure 10. Dynamical *M*/*L* as in Fig. 9, corrected for rotational support and using the Sérsic luminosity profile. Left-hand panel: SIS mass model. Right-hand panel: constant *M*/*L*.

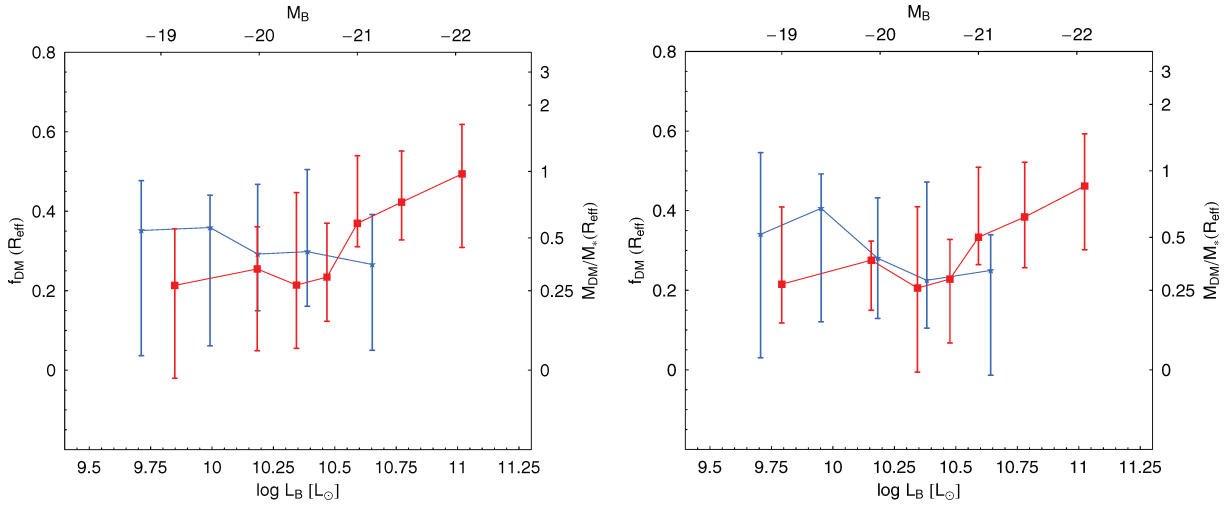

Figure 11. Trends of DM fraction with luminosity, using SIS and constant-*M*/*L* mass models (left- and right-hand panels, respectively). Symbols are as in Figs 9 and 10.

($t_{\rm gal}$, τ, Z) BC03-based stellar population model, and the $\Upsilon_{\rm dyn}$ estimates from the dynamical models using generalized luminosity profiles (Section 4.3). As shown in Fig. 11, $f_{\rm DM}$ increases with luminosity in the E galaxy subsample, but is constant or even *decreasing* for the S0s. The combined ETG sample has $f_{\rm DM}$ increasing overall, but with the hint of a slope change at $M_{\rm B} \sim -20.5$, from roughly constant at faint magnitudes to steeply increasing for brighter objects; the trends for the S0s and the correspondingly fainter Es are roughly consistent. These conclusions are valid for both bracketing mass profile cases (SIS and constant *M*/*L*), although the slope change is less apparent for the SIS model. To quantify this breakdown, we have measured the slopes γ_{DM} of $f_{\rm DM} - L_{\rm B}$ relation for the two models, and found that $\gamma_{\rm DM} \sim 0.5$ for $\log L_{\rm B} \gtrsim 10.4\,{\rm L}_{\odot}$ and $\gamma_{\rm DM} \sim 0$ for $\log L_{\rm B} \lesssim 10.4\,{\rm L}_{\odot}$, clearly inconsistent within the errors.

The trends with luminosity are mirrored by similar correlations with the velocity dispersion as we show in Fig. 12. Here, the slope is steeper in general because of the combined effect of the $\Upsilon_\star$–σ_0 correlation shown in Fig. 7 and the stronger dependence between $\Upsilon_{\rm dyn}$ and σ_0.

The DM fraction is typically $f_{\rm DM} \sim 0.3$ assuming a Salpeter IMF, with a broad range for individual galaxies from ∼0 to ∼0.9 (rms scatter of ∼0.15). About 15 per cent of the galaxies have, within the errors, $f_{\rm DM} < 0$ (typically those with low surface brightness $\mu_{\rm eff}$), an unphysical result which may indicate that the Salpeter IMF is inaccurate (cf. C+06); adopting that a Chabrier IMF would imply more DM, with $f_{\rm DM} \sim 0.6$ typically, and only a tiny handful of galaxies with $f_{\rm DM} < 0$. Changing the IMF also slightly flattens the luminosity dependence of $f_{\rm DM}$, since this quantity is not directly proportional to $\Upsilon_\star$.

We next look for any DM differences between the fast- and slow-rotator Es, following the classification in Section 4.1. However, as shown in Fig. 13, there is no discernible difference; slow and fast rotators typically have $f_{\rm DM} \sim 0.35$ and ∼0.25, respectively, but this is consistent with a simple luminosity effect, since fast rotators are fainter on average than slow rotators. This result appears contrary

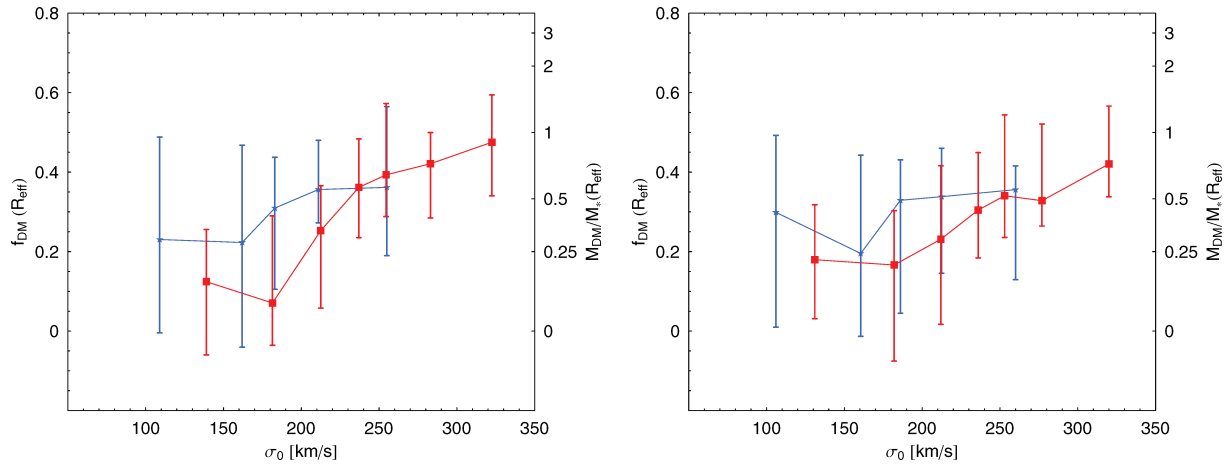

Figure 12. Trends of DM fraction with velocity dispersion, using SIS and constant-*M*/*L* mass models (left- and right-hand panels, respectively). Symbols are as in Figs 9–11.

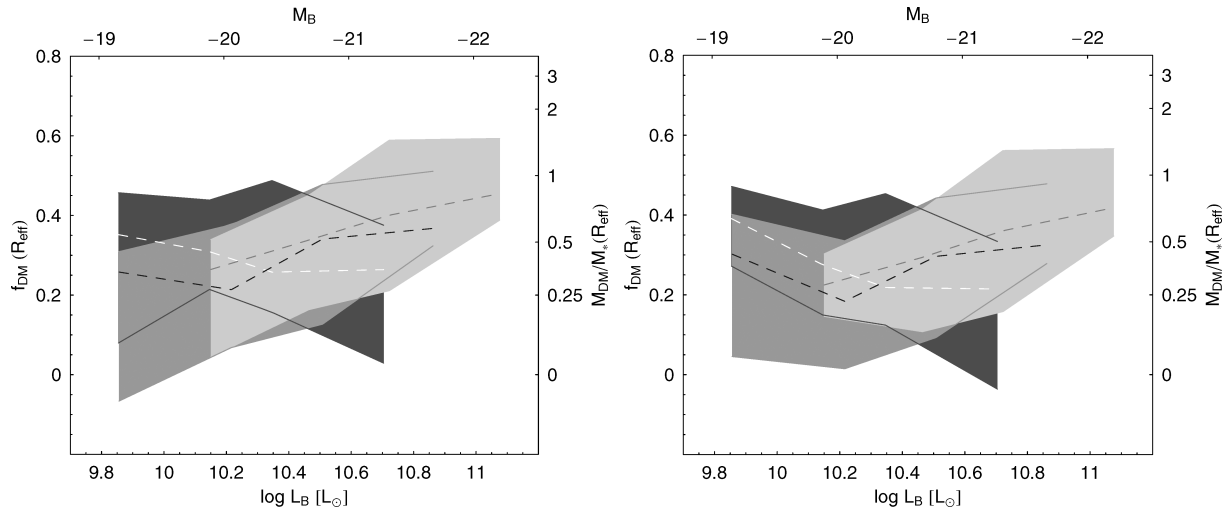

Figure 13. DM fraction trends for different galaxy types, using SIS and constant-*M*/*L* mass models (left- and right-hand panels, respectively). Dashed lines show median binned values and shaded areas show ±25 per cent scatter. Light grey shows slow-rotator Es, medium grey shows fast-rotator Es and dark grey shows S0s.

to the finding of C+06 (based on more detailed dynamical models and somewhat different stellar population constraints for a much smaller galaxy sample) that there is an f_{DM} discontinuity between slow and fast rotators.

We also compare S0s in Fig. 13, where it appears that their declining trend of f_{DM} with luminosity is inconsistent with the Es in the same luminosity range. However, we caution that our spherical dynamical models are most questionable for the S0s, so the overall situation appears consistent with a continuous trend of f_{DM} with luminosity for all ETGs, independent of morphology and rotation. For the rest of this paper, we will therefore generally lump all these ETG subclasses together as one population.

Before continuing further, we check once more the effects of systematic uncertainties, as detailed in Appendix C. Despite the uncertainties, our default model is consistent with results on DM content at larger radii, and we therefore consider the overall mild increase of f_{DM} to be robust, with the inflection at intermediate luminosities perhaps less so.

How do our results compare to previous studies of DM trends in ETG centres? The analysis most similar to ours is from T+04. As discussed in Section 4.3, they found no indication of a correlation between f_{DM} and luminosity, but their sample was primarily of faint galaxies, where we also found that the correlation is weak. If we adopted higher Sérsic indices for the brightest galaxies, the correlation would also weaken for them, but this scenario would seemingly be inconsistent with large-radius tracers of DM (see Appendix C).

Borriello et al. (2003) modelled a large sample of ETGs dynamically and claimed that the flatness of the FP would not permit centrally concentrated DM haloes as predicted by cosmological models. Their results imply $\gamma_\star = 0.27 \pm 0.04$, thereby explaining all the tilt through the stellar populations – in contradiction to our $\gamma_\star = 0.06 \pm 0.01$. This is mainly the consequence of their choice to not allow for a systematic variation of the virial DM fraction with luminosity in their model, and to use homologous $j_\star(r)$ profiles. However, their average f_{DM} (∼0.3) is in broad agreement with our results.

Finally, Padmanabhan et al. (2004) analysed a large sample of SDSS ETGs, using a combination of stellar populations and dynamical models. Although the different redshift ranges make comparisons not straightforward, their results do appear roughly equivalent to ours, with $\gamma_\star \sim 0$ and $\gamma_{dyn} \sim 0.17$, and even a hint of a flattening

of the $f_{\rm DM}$ slope at lower luminosities. Note however that they used an inaccurate homologous $j_\star(r)$ profile.

6 IMPLICATIONS: DARK MATTER AND GALAXY FORMATION

The trends we have seen for $f_{\rm DM}$ as a function of luminosity could provide fresh clues to galaxy formation. The most basic interpretation of central DM variations is that they reflect variations in *total* DM within the virial radius. Assuming that the Universal baryon fraction is roughly conserved from galaxy to galaxy, the implication is then that higher $f_{\rm DM}$ means lower efficiencies of SF $\epsilon_{\rm SF}$. In this respect, the trends we find are qualitatively expected. Both observations and theory point to a universal U-shaped trend of $\epsilon_{\rm SF}$ (or equivalently virial *M*/*L*) with luminosity, and a peak efficiency at $M_\star \sim 10^{11}\,{\rm M}_\odot$ (e.g. Benson et al. 2000; Marinoni & Hudson 2002; N+05; van den Bosch et al. 2007).

Physically, the lowest mass galaxies are least able to retain their primordial gas content long enough to form many stars, since their gravitational potential wells are not deep enough to prevent ejection from supernovae feedback. More massive galaxies are increasingly able to inhibit feedback and form more stars, but at a certain mass scale, additional processes kick in such as active galactic nuclei feedback, inhibiting gas cooling and decreasing $\epsilon_{\rm SF}$ again (e.g. Cattaneo et al. 2006; Shankar et al. 2006; Kaviraj et al. 2007; Tortora et al. 2009). Thus, the lowest mass and the highest mass galaxies are the most DM-dominated. Our current galaxy sample does not extend faint enough to discern any U-shape, but the change we see in the $f_{\rm DM}$ trend below scales of $M_{\rm B} \sim -20.5$ or $M_\star \sim 10^{11}\,{\rm M}_\odot$ does coincide with the generically expected minimum of DM content. The consistencies of the trends for the ETG subtypes (S0s, fast-rotator Es, slow-rotator Es) suggest that the dominant driver of SF is mass, not angular momentum.

It is of course a stretch to draw firm conclusions about virial quantities based on data from scales $\ll R_{\rm eff}$. The central DM content that we are actually probing may be decoupled from the overall DM content in several ways: the central DM density reflects the ambient density at the time of initial halo collapse; the baryons could have interacted with the DM and changed its distribution; and the $f_{\rm DM}$ quantity that we measure is somewhat dependent on the particular values of $R_{\rm eff}$ for the stars rather than simply probing the DM properties. To allow for such effects and to provide quantitative marks for comparison to the cosmological theory, we now consider the properties of the DM alone, in terms of its average density within some small radius, $\langle\rho_{\rm DM}\rangle$.

In order to make critical comparisons with a literature study discussed below, we estimate $\langle\rho_{\rm DM}\rangle$ within 2 $R_{\rm eff}$, extrapolating our usual models outwards in radius. We present this result versus stellar mass for the whole ETG sample in Fig. 14, using a Salpeter IMF and alternatively the SIS or constant-*M*/*L* mass profile. Although these bracketing mass profiles gave similar results for $f_{\rm DM}$ within 1 $R_{\rm eff}$, at 2 $R_{\rm eff}$ they start to diverge more, giving notably different results for $\langle\rho_{\rm DM}\rangle$. The less massive galaxies have increasingly dense DM haloes, apparently reaching a plateau of $\langle\rho_{\rm DM}\rangle \sim 0.05\,{\rm M}_\odot\,{\rm pc}^{-3}$ at masses below $\log M_\star/{\rm M}_\odot \sim 11$.

As a reality check, we compare the results for flattened ETGs in the Coma cluster from Thomas et al. (2009, hereafter T+08), who used detailed three-integral axisymmetric dynamical models of stellar kinematics to decompose the galaxies into their stellar and DM mass components. Their $\langle\rho_{\rm DM}\rangle$ values from their NFW halo model match up remarkably well with our SIS-based results. T+08 fitted their data with a logarithmic density–mass trend which would imply very high central $\langle\rho_{\rm DM}\rangle$ for the faintest galaxies. However, as we can see in the figure, such conclusions would involve extrapolating outside the mass range covered by the data, and in fact the T+08 results do show some sign of the density plateau at small masses which we find.

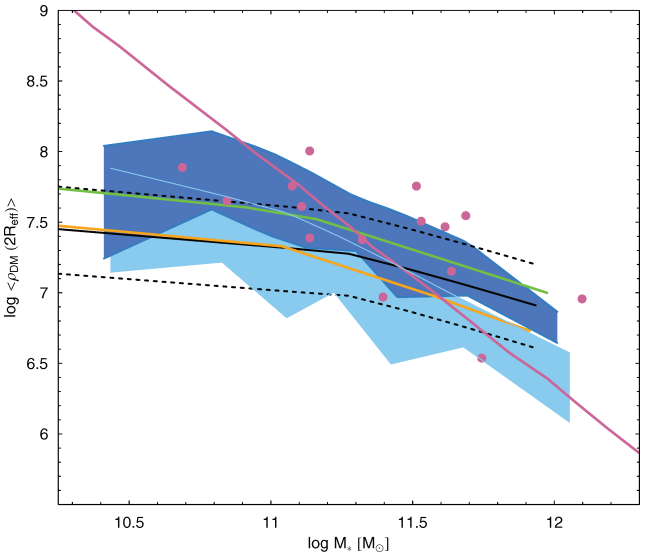

Figure 14. Central DM density in ETGs versus stellar mass. The density is averaged within a radius of 2 $R_{\rm eff}$, and is in units of ${\rm M}_\odot\,{\rm kpc}^{-3}$; a Salpeter IMF is assumed. The 25–75th percentiles are shown as darker and lighter blue for the Sérsic+SIS and const-*M*/*L* models, respectively. Dots are the T+08 galaxy sample with the best fit shown as purple solid line. Orange and green solid lines are the ΛCDM predictions using $\epsilon_{\rm SF} = 60$ and 6 per cent, respectively. The black solid line is the model assuming a varying $\epsilon_{\rm SF}$ (see text for details). The dotted curves represent the range of model predictions due to the scatter in the $R_{\rm eff} - M_\star$ relation.

Now we calculate predictions from Λ cold dark matter (ΛCDM) cosmological models, adopting an NFW density profile, and the Bullock et al. (2001) mass–concentration relation, as discussed in N+05. The final parameter in this model is the mass ratio between stars and DM within the virial radius, taking plausible values of alternatively $M_\star/M_{\rm vir} = 0.1$ or 0.01 (corresponding to $\epsilon_{\rm SF} \sim 6$ or ∼60 per cent, respectively, for a baryon fraction of 0.16; see N+05 and Spergel et al. 2003). The results for $\langle\rho_{\rm DM}\rangle$ are shown in Fig. 14, where the model predictions are seen to be fairly consistent with the observations, including the bend in the $\langle\rho_{\rm DM}\rangle$ trend at similar galaxy masses. This bend is not caused by anything intrinsic to the DM itself, but by the radius adopted for measuring the density. As shown in Fig. 1 (right-hand panel), the mass–$R_{\rm eff}$ relation for ETGs has a bend, which probably explains not only the density trends seen in this section but also the $f_{\rm DM}$ results of the previous section. For bright galaxies, $R_{\rm eff}$ increases rapidly with mass, probing quickly into regions containing more DM, at lower averaged densities. Fainter galaxies have less quickly varying $R_{\rm eff}$ which thus tracks the slowly varying DM scale radius more closely, so that the observable DM properties are roughly constant.

In more detail, the $\epsilon_{\rm SF} = 60$ per cent theoretical case coincides roughly with our observational findings assuming a constant-*M*/*L* profile, and the $\epsilon_{\rm SF} = 6$ per cent case coincides nicely with our SIS-based findings. However, neither of these cases is plausible observationally or theoretically for the full range of galaxy masses. Our final case invokes a transition from high $\epsilon_{\rm SF}$ for the faint galaxies to low $\epsilon_{\rm SF}$ for the bright galaxies, which is generically expected from various lines of evidence. More specifically, motivated by the

findings of N+05 based on radially extended dynamical studies of ETGs (see also e.g. Napolitano et al. 2009a), we assume that the bright galaxies have $\epsilon_{\rm SF}$ decreasing steadily from 60 to 16 per cent in the mass range of $\log M_\star = 11$–$12\,{\rm M}_\odot$; the faint galaxies have a constant $\epsilon_{\rm SF} = 90$ per cent. As shown in Fig. 14, this model would be consistent with our SIS findings at the bright end, and with constant M/L at the faint end. However, the NFW-based models themselves would have roughly SIS profiles for the entire range of luminosity, which means that this set of model assumptions is not self-consistent. It is beyond the scope of this paper to explore the possible combinations of DM parameters that would be fully consistent with the data, but we speculate that the low-luminosity objects have low-concentration DM haloes. Note that changing the IMF to Chabrier would not significantly change these conclusions, since the data curves would shift up and to the left in Fig. 14.

7 CONCLUSIONS

The relative amounts of dark and luminous mass in ETGs are crucial information for understanding the internal structure of these systems and their formation mechanisms. In this paper, we have analysed both the stellar and dynamical M/L in the central regions of one of the largest homogeneous samples of local ETGs, provided by PS96.

We estimate the stellar content by accurate stellar population synthesis models of several observed colours using the BC03 prescription. We measure dynamical masses using the observed central velocity dispersion σ_0 and several simplifying assumptions in the Jeans equations.

We find that the stellar M/L, $\Upsilon_\star$, has a shallow trend with luminosity with a slope $\sim$0.06 for the whole ETG sample (with S0s showing a steeper trend than the Es; see Table 1). Dynamical M/L, on the other hand, has a slope for the $M/L \propto L_{\rm B}^{\gamma}$ relation of 0.21 ± 0.01 when considering ETGs as a (photometrical and kinematical) homologous galaxy family, i.e. fully consistent with results derived in local galaxies' B-band FP.

For the non-homology case (i.e. assuming the Sérsic profile for the light distribution and differential rotation within $R_{\rm eff}$), we find that using the SIS model as the total mass distribution does not much affect the M/L slope and thus not the FP tilt either. On the contrary, non-homology can account for as much as $\sim$40 per cent if considering the constant-M/L model, and even more (up to 80 per cent) for the faint systems.

A further 30 per cent (i.e. 0.06/0.21) is provided by the $\Upsilon_\star$ slope. The residual contribution to the $M/L \propto L_{\rm B}^{\gamma}$ slope ($\sim$70 per cent for the SIS model and 30 per cent for constant M/L) is mainly due to a variation with luminosity of their DM fraction.

It must be stressed that this *average* budget of γ contributions masks a more complicated distribution with luminosity. For instance, for the bright/massive galaxies (i.e. $\log L_{\rm B} \gtrsim 10.4\,{\rm L}_\odot$ and $\log M_\star \gtrsim 11.3\,{\rm M}_\odot$) which have a quasi-$R^{1/4}$ profile and little or no rotation, the effect of the non-homologies is minimal and the slope of the $M/L \propto L_{\rm B}^{\gamma}$ remains steeper than the faint systems where non-homologies can account for almost all the slope γ. This, obviously, relates to the trend of the DM fractions discussed in Section 5.

Here, we have seen that $f_{\rm DM}$ is strongly varying with luminosity and mass. In particular, we observe a dichotomy in DM content of bright and faint Es: galaxies brighter than $M_{\rm B} \sim -20.5$ and more massive than $\log M_\star \sim 11$–$11.3\,{\rm M}_\odot$ have an increasingly larger $f_{\rm DM}$, while galaxies lying below these luminous and mass scales invert the trend, such that $f_{\rm DM}$ is constant or marginally decreasing with luminosity and mass. When separating the E sample into 'slow' and 'fast' rotators, it is evident that this two-fold trend is mainly found in the fast-rotator systems (see Fig. 13). These two kinematical varieties do not show large differences in their $f_{\rm DM}$ properties. In particular, we do not find significant evidence for systematically lower $f_{\rm DM}(R_{\rm eff})$ for the fast-rotator variety (C+06), although with a large scatter one might make such a conclusion using a small statistical sample. The inclusion of the ellipticity and orbital anisotropy would increase the steepness of the faint/less massive sample, but would leave the bright/massive galaxy range unaffected, still maintaining the dichotomy (Fig. C1, bottom-right panel). As an alternative to a variable DM content, we have briefly analysed the effect of a change of IMF as a function of luminosity (see Fig. 6), which could also explain the FP tilt.

The $f_{\rm DM}$ dichotomy adds to other well-known ETG correlations as found in the $\mu_e - R_{\rm eff}$ relation, FJ, size–luminosity (or size–mass) relations and in the correlations of Sérsic index with both galaxy size and luminosity, as discussed in Sections 2, 3.2 and 4 (Capaccioli et al. 1992; Prugniel & Simien 1997; Shen et al. 2003; Matković & Guzmán 2005, etc.). Our results mirror the DM content in the outskirts of galaxies, where variations of virial M/L as a function of mass and luminosity have been found both in simulations and in observational analysis (Benson et al. 2000; Marinoni & Hudson 2002; van den Bosch et al. 2007). A similar dichotomy in DM content is not observed for S0s, which are generally fainter and less massive than Es and are strongly affected by rotational support (influencing the normalization of $\Upsilon_{\rm dyn}$). They have a slightly higher DM fraction and show a monotonically decreasing trend with mass and luminosity, consistent with what is known for spiral galaxies (Persic, Salucci & Ashman 1993).

A continuity in DM content of galaxy as a function of amount of rotational support is possibly shown in Fig. 13, where we plot DM fractions as a function of luminosity for slow and fast rotators and lenticulars.

Looking at the average central DM density, $\langle\rho_{\rm DM}\rangle$, we have found that this quantity has a fairly small scatter within the ETG sample. Albeit model-dependent – the Sérsic+SIS model providing $\langle\rho_{\rm DM}\rangle$ which are 0.2–0.4 dex larger than the ones obtained with the constant M/L – the overall trend of the galaxy distribution decreases monotonically with the stellar mass and luminosity in good agreement with independent results obtained by T+08 for ellipticals in the Coma cluster. Our larger statistical sample, though, has allowed us to discern the presence of a 'knee' in the distribution (around the usual mass/luminosity scale at $\log M_\star \sim 11\,{\rm M}_\odot$ and $\log L_{\rm B} \sim 10.4\,{\rm L}_\odot$) where the relation of the more massive/luminous galaxies bends to a steeper slope than the one followed by the less massive/luminous systems. We have shown that this 'knee' can be explained with the change of the slope in the $R_{\rm eff} - M_\star$ relation at $\log M_\star \sim 11\,{\rm M}_\odot$.

As a robust estimator of the central DM density, $\langle\rho_{\rm DM}\rangle$ can be compared against the expected values for standard NFW profiles. The match found is broadly good, with the results obtained assuming the Sérsic+SIS model favouring high dark-to-luminous mass ratios, i.e. lower SF efficiencies, while the constant-M/L models fit lower $M_{\rm vir}/M_\star$ values, i.e. higher efficiencies. In order to match up with the picture where galaxies have SF efficiencies varying with the stellar mass (Benson et al. 2000; Dekel & Birnboim 2006), we have shown that the DM density characteristics should change with the mass with low-mass systems being surrounded by more 'cored' haloes (well approximated by the constant-M/L models) and high-mass systems by 'cusped' haloes (here reproduced by the Sérsic+SIS profile).

This *DM non-homology* could be a possible explanation of the 'anomalously' low-halo-concentration parameters recently found

modelling intermediate luminosity galaxies, compared to the giant ellipticals showing 'regular' concentration as expected from the ΛCDM simulations (Napolitano et al., in preparation). In this respect, a model like the Einasto profile (Einasto 1965, but see also Navarro et al. 2004, 2008; Cardone, Piedipalumbo & Tortora 2005; Graham et al. 2006) or a phenomenological model including a wide range of innermost density slopes (Tortora et al. 2007) provides suitable working hypotheses to test on larger data sample with extended kinematics (e.g. Atlas3D;[16] or the PN.S Elliptical Galaxy Survey: Douglas et al. 2007; Coccato et al. 2009; Napolitano et al. 2009a).

ACKNOWLEDGMENTS

We thank the anonymous referee for his/her kind report. We also thank Michele Cappellari for fruitful discussions and Claudia Maraston for providing us with her synthetic spectral models. NRN was funded by CORDIS within FP6 with a Marie Curie European Reintegration Grant, contract no. MERG-FP6-CT-2005-014774, co-funded by INAF. AJR was supported by the National Science Foundation Grants AST-0507729 and AST-0808099. CT was supported by a grant from the project Mecenass, funded by the Compagnia di San Paolo.

REFERENCES

Aceves H., Velázquez H., 2005, MNRAS, 360, L50
Almeida C., Baugh C. M., Lacey C. G., 2007, MNRAS, 376, 1711
Bekki K., 1998, ApJ, 496, 713
Bell E. F., de Jong R. S., 2001, ApJ, 550, 212B (BdJ01)
Bell E. F., McIntosh D. H., Katz N., Weinberg M. D., 2003, ApJS, 149, 289
Benson A. J., Cole S., Frenk C. S., Baugh C. M., Lacey C. G., 2000, MNRAS, 311, 793
Bernardi M. et al., 2003, AJ, 125, 1849
Bernardi M., Hyde J. B., Sheth R. K., Miller C. J., Nichol R. C., 2007, AJ, 133, 1741
Bertin G., Ciotti L., Del Principe M., 2002, A&A, 386, 149
Bolton A. S., Burles S., Treu T., Koopmans L. V. E., Moustakas L. A., 2007, ApJ, 665, L105
Bolton A. S., Treu T., Koopmans L. V. E., Gavazzi R., Moustakas L. A., Burles S., Schlegel D. J., Wayth R., 2008, ApJ, 684, 248
Borriello A., Salucci P., Danese L., 2003, MNRAS, 341, 1109
Boylan-Kolchin M., Ma C.-P., Quataert E., 2005, MNRAS, 362, 184
Boylan-Kolchin M., Ma C.-P., Quataert E., 2006, MNRAS, 369, 1081
Bruzual G., 2007, in Vallenari A., Tantalo R., Portinari L., Moretti A., eds, ASP Conf. Ser. Vol. 374, From Stars to Galaxies: Building the Pieces to Build Up the Universe. Astron. Soc. Pac., San Francisco, p. 303
Bruzual A. G., Charlot S., 2003, MNRAS, 344, 1000 (BC03)
Bullock J. S., Kolatt T. S., Sigad Y., Somerville R. S., Kravtsov A. V., Klypin A. A., Primack J. R., Dekel A., 2001, MNRAS, 321, 559
Busarello G., Capaccioli M., Capozziello S., Longo G., Puddu E., 1997, A&A, 320, 415
Burkert A., 1995, ApJ, 447, 25
Caon N., Capaccioli M., D'Onofrio M., 1993, MNRAS, 265, 1013
Capaccioli M., Caon N., D'Onofrio M., 1992, MNRAS, 259, 323
Capaccioli M., Napolitano N. R., Arnaboldi M., 2002, Proc. Sakharov Conf. of Physics, in press (astro-ph/0211323)
Capelato H. V., de Carvalho R. R., Carlberg R. G., 1995, ApJ, 451, 525
Cappellari M. et al., 2006, MNRAS, 366, 1126 (C+06)
Cappellari M. et al., 2007, MNRAS, 379, 418
Cardone V. F., Piedipalumbo E., Tortora C., 2005, MNRAS, 358, 1325
Cattaneo A., Dekel A., Devriendt J., Guiderdoni B., Blaizot J., 2006, MNRAS, 370, 1651
Chabrier G., 2001, ApJ, 554, 1274
Chabrier G., 2001, ApJ, 567, 304
Chabrier G., 2003, PASP, 115, 763
Chiosi C., Carraro G., 2002, MNRAS, 335, 335
Coccato L. et al., 2009, MNRAS, 394, 1249
Conroy C., Gunn J. E., White M., 2008, ApJ, submitted (arXiv:0809.4261)
Covone G. et al., 2009, ApJ, 691, 531
Dantas C. C., Capelato H. V., Ribeiro A. L. B., de Carvalho R. R., 2003, MNRAS, 340, 398
Davé R., 2008, MNRAS, 385, 147
Dekel A., Birnboim Y., 2006, MNRAS, 368, 2
Dekel A., Cox T. J., 2006, MNRAS, 370, 1445
De Lucia G., Springel V., White S. D. M., Croton D., Kauffmann G., 2006, MNRAS, 366, 499D
Desroches L.-B., Quataert E., Ma C.-P., West A. A., 2007, MNRAS, 377, 402
de Vaucouleurs G., 1948, Ann. d' Ap., 11, 247
de Vaucouleurs G., de Vaucouleurs A., Corwin H. G., Buta R. J., Paturel G., Fouque P., 1991, Third Reference Catalogue of Bright Galaxies. Springer-Verlag, New York (RC3)
di Serego Alighieri S., Lanzoni B., Jørgensen I., 2006, ApJ, 647, L99
Djorgovski S., Davis M., 1987, ApJ, 313, 59D
D'Onofrio M., Valentinuzzi T., Secco L., Caimmi R., Bindoni D., 2006, New Astron. Rev., 50, 447
D'Onofrio M. et al., 2008, ApJ, 685, 875
Douglas N. G. et al., 2007, ApJ, 664, 257
Dressler A., Lynden-Bell D., Burstein D., Davies R. L., Faber S. M., Terlevich R., Wegner G., 1987, ApJ, 313, 42D
Einasto J., 1965, Trudy Inst. Astroz. Alma-Ata, 51, 87
Eke V., et al. (2dF team), 2004, MNRAS, 348, 866
Eminian C., Kauffmann G., Charlot S., Wild V., Bruzual G., Rettura A., Loveday J., 2008, MNRAS, 384, 930
Emsellem E. et al., 2004, MNRAS, 352, 721
Evstigneeva E. A., de Carvalho R. R., Ribeiro A. L., Capelato H. V., 2004, MNRAS, 349, 1052
Faber S. M., Jackson R. E., 1976, ApJ, 204, 668F (FJ)
Ferreras I., Silk J., 2000, MNRAS, 316, 786
Ferreras I., Saha P., Williams L. L. R., 2005, ApJ, 623, L5
Ferreras I., Saha P., Burles S., 2008, MNRAS, 383, 857
Ferrarese L., Merritt D., 2000, ApJ, 539, L9
Fioc M., Rocca-Volmerange B., 1997, A&A, 326, 950
Forbes D., Lasky P., Graham A., Spitler L., 2008, MNRAS, 389, 1924
Gargiulo A. et al., 2009, MNRAS, in press (doi:10.1111/j.1365-2966.2009.14801.x) (arXiv:0902.4383)
Gavazzi G., Bonfanti C., Sanvito G., Boselli A., Scodeggio M., 2002, ApJ, 576, 135G
Gavazzi R., Treu T., Rhodes J. D., Koopmans L. V. E., Bolton A. S., Burles S., Massey R. J., Moustakas L. A., 2007, ApJ, 667, 176
Gebhardt K. et al., 2003, ApJ, 583, 92
Gerhard O., Kronawitter A., Saglia R., Bender R., 2001, AJ, 121, 1936 (G+01)
González-García A. C., van Albada T. S., 2003, MNRAS, 342, L36
Graham A. W., 1998, MNRAS, 295, 933
Graham A., Colless M., 1997, MNRAS, 287, 221
Graham A. W., Guzmán R., 2003, AJ, 125, 2936
Graham A. W., Merritt D., Moore B., Diemand J., Terzić B., 2006, AJ, 132, 2701
Graves G. J., 2009, PhD thesis, Univ. California
Hernquist L., 1990, ApJ, 356, 359
Hjorth J., Madsen J., 1995, ApJ, 445, 55
Hopkins P. F., Cox T. J., Hernquist L., 2008, ApJ, 689, 17
Hyde J. B., Bernardi M., 2009a, MNRAS, 394, 1978
Hyde J. B., Bernardi M., 2009b, MNRAS, in press (doi:10.1111/j.1365-2966.2009.14783.x) (arXiv:0810.4924)
Jensen J. B., Tonry J. L., Barris B. J., Thompson R. I., Liu M. C., Rieke M. J., Ajhar E. A., Blakeslee J. P., 2003, ApJ, 583, 712
Jorgensen I., Franx M., Kjaergaard P., 1993, ApJ, 411, 34
Jun H. D., Im M., 2008, ApJ, 678, L97

[16] http://www-astro.physics.ox.ac.uk/atlas3d/

Kannappan S. J., Gawiser E., 2007, ApJ, 657, 5
Kaviraj S., Kirkby L. A., Silk J., Sarzi M., 2007, MNRAS, 382, 960
Kochanek C. S., 1991, ApJ, 373, 354
Kochanek C. S. et al., 2000, ApJ, 543, 131
Koopmans L. V. E., Treu T., Bolton A. S., Burles S., Moustakas L. A., 2006, ApJ, 649, 599
Kormendy J., 1977, ApJ, 218, 333
Kormendy J., Fisher D. B., Cornell M. E., Bender R., 2009, ApJS, 182, 216
Kritsuk A. G., 1997, MNRAS, 284, 327
Kroupa P., 2001, MNRAS, 322, 231
Kronawitter A., Saglia R. P., Gerhard O., Bender R., 2000, A&AS, 144, 53
La Barbera F., Busarello G., Merluzzi P., de la Rosa I., Coppola G., Haines C. P., 2008, ApJ, 689, 913
Lauer T. R. et al., 2007, ApJ, 662, 808
Levine S. E., Aguilar L. A., 1996, MNRAS, 280, L13
Lintott C. J., Ferreras I., Lahav O., 2006, ApJ, 648, 826
McGrath E. J., Stockton A., Canalizo G., 2007, ApJ, 669, 241
Magorrian J. et al., 1998, AJ, 115, 2285
Mamon G. A., Łokas E. L., 2005, MNRAS, 362, 95
Maraston C., 2005, MNRAS, 362, 799 (M05)
Maraston C., Daddi E., Renzini A., Cimatti A., Dickinson M., Papovich C., Pasquali A., Pirzkal N., 2006, ApJ, 652, 85
Marinoni C., Hudson M. J., 2002, ApJ, 569, 101
Mathews W. G., Brighenti F., 2000, ApJ, 545, 181
Matković A., Guzmán R., 2005, MNRAS, 362, 289
Mobasher B., Guzman R., Aragon-Salamanca A., Zepf S., 1999, MNRAS, 304, 225
Napolitano N. R., Arnaboldi M., Freeman K. C., Capaccioli M., 2001, A&A, 377, 784
Napolitano N. R. et al., 2005, MNRAS, 357, 691 (N+05)
Napolitano N. R. et al., 2008, in Davies J. I., Disney M. J., eds, Proc. IAU Symp. 244, Dark Galaxies & Lost Baryons. Cambridge Univ. Press, Cambridge, p. 289
Napolitano N. R. et al., 2009a, MNRAS, 393, 329
Navarro J. F., Frenk C. S., White S. D. M., 1996, ApJ, 462, 563
Navarro J. F., Frenk C. S., White S. D. M., 1997, ApJ, 490, 493
Navarro J. F., Hayashi E., Power C., Jenkins A. R., Frenk C. S., 2004, MNRAS, 349, 1039
Navarro J. F. et al., 2008, MNRAS, submitted (arXiv:0810.1522)
Nigoche-Netro A., Ruelas-Mayorga A., Franco-Balderas A., 2008, A&A, 491, 731
Nipoti C., Londrillo P., Ciotti L., 2002, MNRAS, 332, 901
Nipoti C., Londrillo P., Ciotti L., 2003, MNRAS, 342, 501
Noeske K. G. et al., 2007, ApJ, 660, L47
Oñorbe J., Domínguez-Tenreiro R., Sáiz A., Serna A., Artal H., 2005, ApJ, 632, L57
Oñorbe J., Domínguez-Tenreiro R., Sáiz A., Artal H., Serna A., 2006, MNRAS, 373, 503
Padmanabhan N. et al., 2004, New Astron., 9, 329
Pahre M. A., Djorgovski S. G., de Carvalho R. R., 1995, ApJ, 453, L17
Pahre M. A., Djorgovski S. G., de Carvalho R. R., 1998a, AJ, 116, 1591
Pahre M. A., de Carvalho R. R., Djorgovski S. G., 1998b, AJ, 116, 1606
Persic M., Salucci P., Ashman K. M., 1993, A&A, 279, 343
Press W. H., Teukolsky S. A., Vetterling W. T., Flannery B. P., 1992, Numerical Recipes in C, 2nd edn. Cambridge Univ. Press, Cambridge
Proctor R. N., Lah P., Forbes D. A., Colless M., Couch W., 2008, MNRAS, 386, 1781
Prugniel P., Simien F., 1996, A&A, 309, 749 (PS96)
Prugniel P., Simien F., 1997, A&A, 321, 111 (PS97)
Reda F. M., Forbes D. A., Hau G. K. T., 2005, MNRAS, 360, 693
Renzini A., Ciotti L., 1993, ApJ, 416, L49
Rettura A. et al., 2006, A&A, 458, 717
Riciputi A., Lanzoni B., Bonoli S., Ciotti L., 2005, A&A, 443, 133
Robertson B., Cox T. J., Hernquist L., Franx M., Hopkins P. F., Martini P., Springel V., 2006, ApJ, 641, 21
Romanowsky A. J., Douglas N. G., Arnaboldi M., Kuijken K., Merrifield M. R., Napolitano N. R., Capaccioli M., Freeman K. C., 2003, Sci, 301, 1696
Romanowsky A. J. et al., 2008, AJ, submitted (arXiv:0809.2988)
Romeo A. D., Napolitano N. R., Covone G., Sommer-Larsen J., Antonuccio-Delogu V., Capaccioli M., 2008, MNRAS, 389, 13
Salpeter E. E., 1955, ApJ, 121, 161
Scalo J. M., 1986, Fundam. Cosmic Phys., 11, 1
Scodeggio M., Gavazzi G., Belsole E., Pierini D., Boselli A., 1998, MNRAS, 301, 1001
Sérsic J. L., 1968, Atlas de Galaxies Australes. Observatorio Astronomico de Cordoba, Cordoba
Shankar F., Lapi A., Salucci P., De Zotti G., Danese L., 2006, ApJ, 643, 14
Schuberth Y., Richtler T., Dirsch B., Hilker M., Larsen S. S., Kissler-Patig M., Mebold U., 2006, A&A, 459, 391
Schwarzschild M., 1979, ApJ, 232, 236
Shen S., Mo H. J., White S. D. M., Blanton M. R., Kauffmann G., Voges W., Brinkmann J., Csabai I., 2003, MNRAS, 343, 978
Spergel D. N. et al., 2003, ApJS, 148, 175
Teodorescu A. M., Méndez R. H., Saglia R. P., Riffeser A., Kudritzki R.-P., Gerhard O. E., Kleyna J., 2005, ApJ, 635, 290
Thomas D., Maraston C., Bender R., Mendes de Oliveira C., 2005, ApJ, 621, 673
Thomas J., Saglia R. P., Bender R., Thomas D., Gebhardt K., Magorrian J., Corsini E. M., Wegner G., 2009, ApJ, 691, 770 (T+08)
Tonry J. L., Dressler A., Blakeslee J. P., Ajhar E. A., Fletcher A. B., Luppino G. A., Metzger M. R., Moore C. B., 2001, ApJ, 546, 681
Tortora C., Cardone V. F., Piedipalumbo E., 2007, A&A, 463, 105
Tortora C., Antonuccio-Delogu V., Kaviraj S., Silk J., Romeo A. D., Becciani U., 2009, MNRAS, in press (doi:10.1111/j.1365-2966.2009.14718.x) (arXiv:0903.0397)
Trager S. C., Faber S. M., Worthey G., González J. J., 2000, AJ, 120, 165
Trujillo I., Burkert A., Bell E. F., 2004, ApJ, 600, L39 (T+04)
van den Bosch F. C. et al., 2007, MNRAS, 376, 841
van der Marel R. P., 1991, MNRAS, 253, 710
van der Marel R. P., van Dokkum P. G., 2007, ApJ, 668, 756 (MD07)
van Dokkum P. G., 2008, ApJ, 674, 29
van Dokkum P. G., van der Marel R. P., 2007, ApJ, 655, 30
Vazdekis A., Casuso E., Peletier R. F., Beckman J. E., 1996, ApJS, 106, 307
Weijmans A.-M., Krajnović D., van de Ven G., Oosterloo T. A., Morganti R., de Zeeuw P. T., 2008, MNRAS, 383, 1343
Zaritsky D., Gonzalez A. H., Zabludoff A. I., 2006, ApJ, 638, 725

APPENDIX A: SYSTEMATIC EFFECTS IN THE STELLAR POPULATION MODELS

Here, we examine the role of systematic uncertainties in the stellar population results, using different assumptions and basis models (see also similar analysis in Rettura et al. 2006; Kannappan & Gawiser 2007; Conroy, Gunn & White 2008). First, we consider our default model based on BC03, using three different parametrizations for the SFH. In our reference model, τ and Z (as well as $t_{\rm gal}$) are free parameters fitted to each galaxy; a more simplified model has fixed $\tau = 0.75$ Gyr and $Z = Z_{\odot}$ corresponding to typical values for the whole sample; an even simpler SSP model has $\tau = 0$ and $Z = Z_{\odot}$. As shown in Fig. A1 (left-hand panel), the distributions of $\Upsilon_{\star}$ in all these models are fairly similar, except in the simplest case which shows a stronger tail to low values of $\Upsilon_{\star}$. The impact of these differences is shown in Fig. A2 (left-hand panel), where it can be seen that overly restrictive modelling assumptions compensate with large variations in $\Upsilon_{\star}$ and thus steeper values for $\gamma_{\star}$.

Next we compare basis model variations, starting with BC03 and M05. The different input stellar models and treatments of the thermally pulsing asymptotic giant branch (TP-AGB) phase lead to different $\Upsilon_{\star}$ predictions for the same colours (Maraston et al.

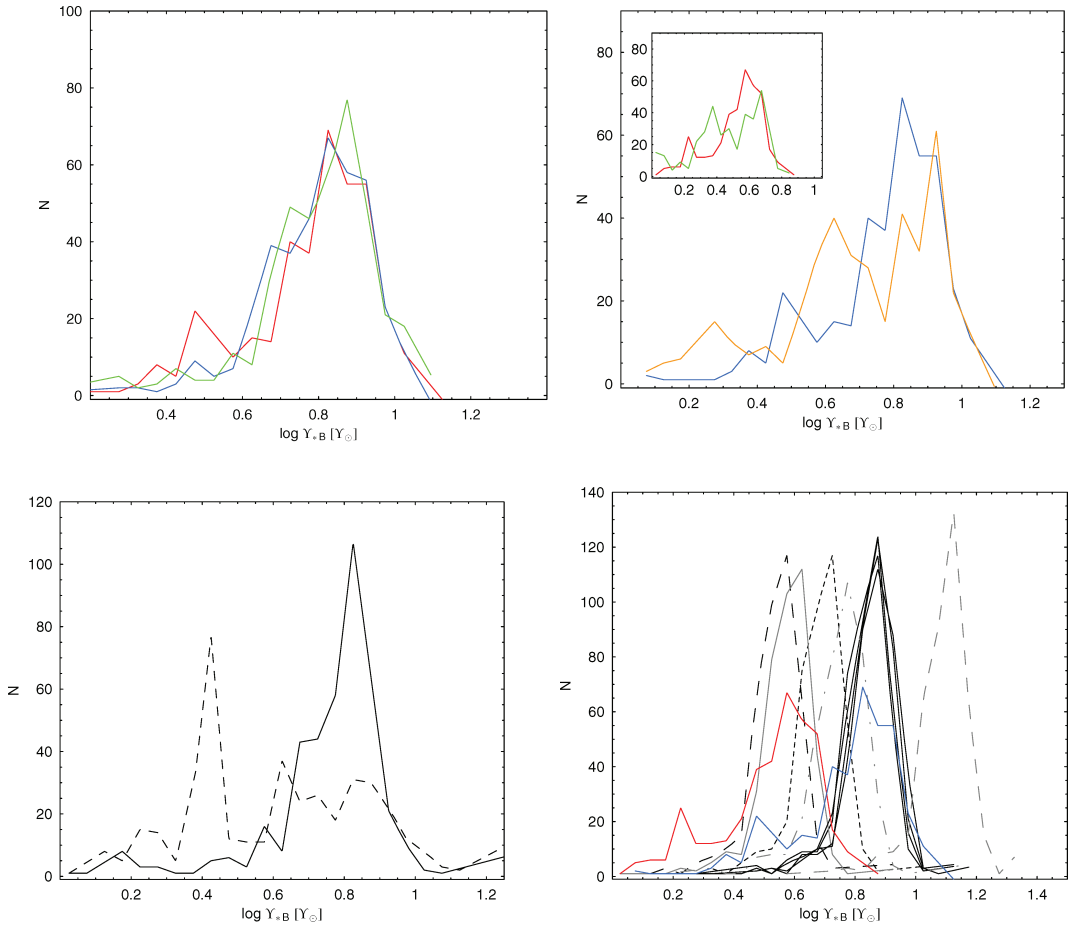

Figure A1. Distributions of recovered $\Upsilon_{*,B}$ from PS96 galaxy sample, for different stellar population models and assumptions. Top-left panel: BC03+Salpeter model with different parameter assumptions: $\tau = 0$ and $Z = Z_{\odot}$ (red); $\tau = 0.75$ Gyr and $Z = Z_{\odot}$ (blue); and τ and Z free to vary (green). Top-right panel: BC03 and M05 models compared, assuming $\tau = 0$ and $Z = Z_{\odot}$. The main panel shows a Salpeter IMF, with BC03 in blue and M05 in orange; the inset panel shows a lower mass IMF, with BC03+Chabrier in red and M05+Kroupa in green. Bottom-left panel: BC03 and M05 models compared (solid and dashed lines, respectively), with Z free to vary. Bottom-right panel: BC03 and BdJ01 models compared, assuming $\tau = 0$ and $Z = Z_{\odot}$. The solid black lines show BdJ01, and blue shows BC03, in both cases with a Salpeter IMF. Lower mass IMFs are also shown: red is BC03 with Chabrier IMF, short-dashed black is BdJ01 with 'scaled' Salpeter IMF, long-dashed black is BdJ01 with 'modified' Salpeter IMF, solid dark grey is BdJ01 with Scalo IMF, dashed light grey is BdJ01 with 'top-light' IMF slope and dot–dashed light grey is BdJ01 with 'top-heavy' IMF slope (the latter two cases using the PEGASE prescription).

2006).[17] Comparisons of some parameters derived from the two models with solar metallicity, given the same colour data, are made in Fig. A2 (right-hand panels). The inferred ages agree very well for older populations, with M05 returning ages up to ∼10 per cent higher than BC03, while for younger populations, up to ∼30 per cent lower. The difference stems from M05 predicting $V - R$ and $V - I$ to be redder for young populations and bluer for old, while $B - V$ is redder for all ages. The implications for $\Upsilon_{\star}$ are that agreement is good for $\Upsilon_{\star} \gtrsim 6\Upsilon_{\odot}$, while for lower values the M05 predictions are smaller by up to a factor of 2. The extension of the M05 results to smaller values of $\Upsilon_{\star}$ can also be seen in Fig. A1. The final impact of these systematic differences on the trend of $\Upsilon_{\star}$ with luminosity is shown in Fig. A2 (left-hand panel): M05 yields a more steeply increasing trend.

We finally examine the SSP models from BdJ01. BdJ01 predict a tight correlation between $\Upsilon_{\star}$ and galaxy colours:[18] using relations for the three colours $B - V$, $B - R$ and $V - I$ and minimizing a χ^2 function, we determine the best-fitted $\Upsilon_{\star}$ for the BdJ01 prescriptions which are shown in Fig. A1 (bottom right-hand panel).

Assuming a Salpeter IMF, the use of different stellar prescriptions (BC03 versus BdJ01) has a negligible effect on the bulk of the $\Upsilon_{\star}$ distribution (e.g. solid black lines and blue ones in the figure). Some of the assumed IMFs in BdJ01 ('scaled' and 'modified' Salpeter and the Scalo (1986), for further details see BdJ01) predict lower $\Upsilon_{\star}$, with the scaled Salpeter and Scalo IMFs giving similar results of the BC03+Chabrier one (red curves in the same figure). Finally, using BdJ01 results for PEGASE (Fioc & Rocca-Volmerage 1997) prescription we obtain that (1) a top-heavy IMF with a slope −0.85

[17] Recent preliminary updates of the BC03 models have included an improved TP-AGB phase treatment (Bruzual 2007; Eminian et al. 2008). The colours and $\Upsilon_{\star}$ predictions are altered, particularly in the near-infrared, but not substantially for $Z \geq 0.4\,Z_{\odot}$. These new models are more similar to M05 than BC03 but for old ages resemble BC03 (McGrath, Stockton & Canalizo 2007).

[18] This was obtained for spiral galaxies but it has been proven to work for ETGs as well (BdJ01; Bell et al. 2003).

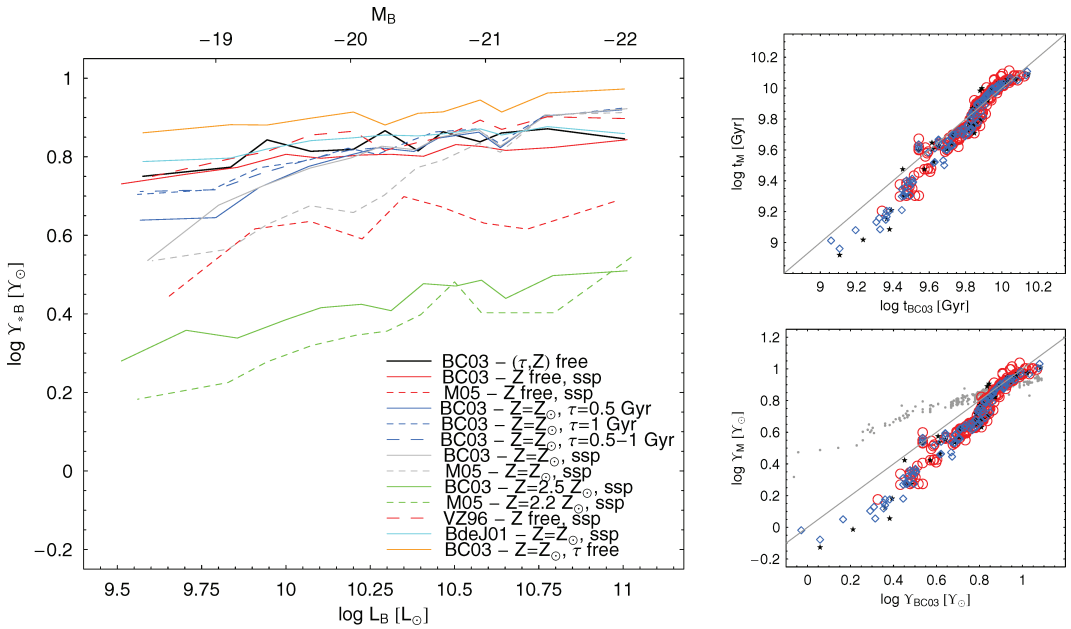

Figure A2. Left-hand panel: median binned stellar *M*/*L* as a function of luminosity, for our ETG sample and under various modelling assumptions. Different stellar population prescriptions are shown (VZ96; BdJ01; BC03; M05), as well as different parameter assumptions – see figure legend for details. Right-hand panels: comparisons of model parameters derived from the same data using different basis population models. The top-right panel shows the age, and the bottom-right panel is stellar *M*/*L*, with the horizontal axes providing the results from BC03 models, and the vertical axes M05 results – in both cases assuming a Salpeter IMF. The red circles are E galaxies, blue diamonds are S0s and black stars are galaxies of other classifications not used in our main study. Solid lines show the one-to-one consistency relation. Grey squares in the bottom-right panel show BdJ01 modelling results.

gives $\Upsilon_\star$ values which are in between of the Kroupa (2001) IMF (or Chabrier or Scalo) and Salpeter IMF predictions, while (2) a top-light IMF with a slope −1.85 give much larger $\Upsilon_\star$ values. Note that distributions using directly BC03 (red and blue lines in left-hand panel of Fig. A1) have a larger spread around the peak distribution than the BdJ01 results.

BdJ01 results have been plotted in bottom right-hand panel of Fig. A2 like grey points. The slope of the relation shown in this figure is unchanged if we use the various prescriptions analysed in the paper above (see distributions using a Salpeter IMF in bottom right-hand panel of Fig. A1); on the contrary, a little change in the zero-point is observed.

As a final test, we compare results using different models *and data* on the same galaxies. As a stellar synthesis model, C+06 fit single burst models (using stellar prescription in Vazdekis et al. 1996) to some line-strength indices. Their estimates are on average 20 per cent larger than ours (with a scatter of 17 per cent). This discrepancy could not be fixed by fitting Vazdekis et al. (1996) or BC03 SSP models to our galaxy colours. Some systematics can be ascribed, partially, to the extrapolation of line-strength indices (and velocity dispersion) from the very central regions to the effective radius, if some change in the average stellar population is present and unaccounted.

APPENDIX B: INDEPENDENT CHECKS ON DYNAMICAL MASSES

Given the simplifications of our Jeans models used to derive the dynamical masses (spherical quasi-isotropic models), we test here using independent results whether our methods have introduced any systematic bias for $\Upsilon_{\rm dyn}$. Our first crosscheck is with C+06, who constructed detailed two-dimensional models of nearby ETGs. Our sample has 18 galaxies in common with theirs.[19] The main differences between the two data sets are (1) our distance moduli are on average larger (0.05 mag) than C+06 but consistent within the scatter, (2) our effective radii are on average 5 per cent larger with a median scatter of 16 per cent and (3) the central velocity dispersions from C+06 are lower than the PS96 values by 6 ± 15 km s^{-1} (see Emsellem et al. 2004).

C+06 constructed flattened, axisymmetric, constant-*M*/*L* dynamical models, using both two-integral Jeans models and three-integral Schwarzschild (1979) orbit models. Their luminosity models are multi-Gaussian expansions of the observed surface brightness profiles, and thus quite non-homologous. Converting our constant-*M*/*L* Sérsic-based $\Upsilon_{\rm dyn}$ results to the *I* band and to the C+06 distances, we compare to their results in Fig. B1. The masses are broadly consistent, with a systematic trend for ours to be higher by ∼20 per cent.

There are several possible reasons for this residual discrepancy, including rotation, orbital anisotropy variations and galaxy flattening – all of which were handled in rigorous detail by C+06 but not by our models. Based on the results of Cappellari et al. (2007), the anisotropy effect should not correlate strongly with luminosity, but rotation and flattening probably do. We also compare our *modelled* values of σ_e (the velocity dispersion integrated over a 1 $R_{\rm eff}$ aperture, folding in the rotational contribution) with their *observed* values, to see if our extrapolation from the central aperture could be generating the discrepancy. However, our σ_e values turn out to

[19] Another seven from their sample did not have measured $B - I$ colours available for making a proper comparison between their *I*-band and our *B*-band $\Upsilon_{\rm dyn}$ results.

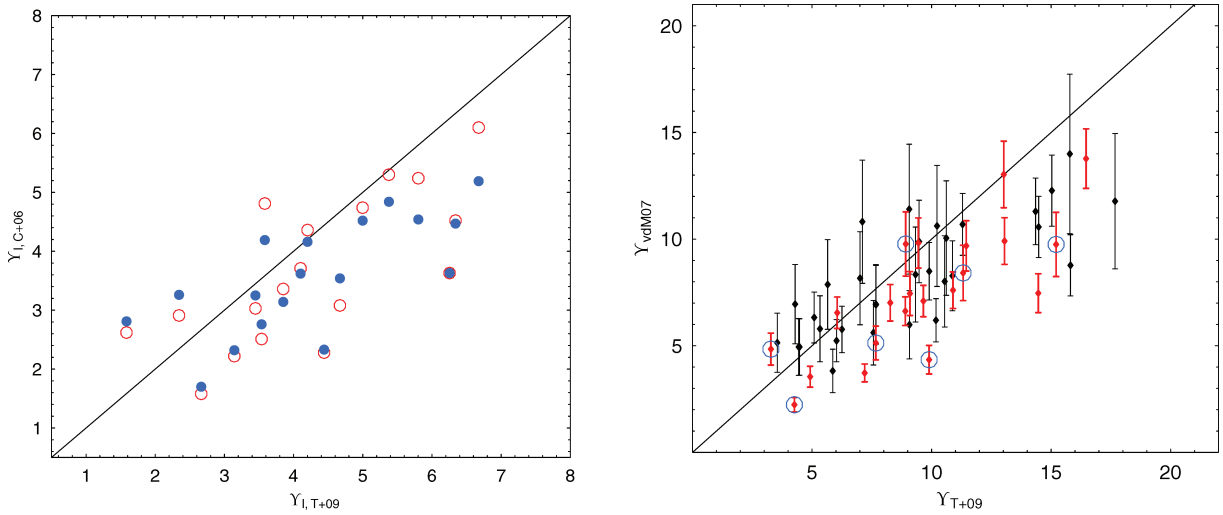

Figure B1. Comparison of dynamical *M*/*L* estimates from our models (horizontal axes) and those from the literature (vertical axes). The diagonal lines show the one-to-one relation. Left-hand panel: comparison to C+06 results in the *I* band. Open red and filled blue symbols are for three-integral Schwarzschild and two-integral Jeans dynamical models, respectively. Right-hand panel: comparison to MD07 results in the *B* band. Red symbols represent galaxies with results including C+06; blue circles show those based solely on data from C+06 also, while those with blue circles use only results from C+06.

be *lower* by 13^{+9}_{-8} km s^{-1}, which goes the wrong way to explain our *higher* masses.

Next we consider the detailed spherical dynamical models of G+01, with 16 galaxies in common. After shifting to the same distance scale, our $\Upsilon_{\rm dyn}$ values at $R_{\rm eff}$ are 27 ± 8 per cent *lower* on average than theirs. Since their sample was focused on round galaxies, we suspect again that flattening is playing a key role in the accuracy of our results, but that we have been able to largely compensate for its effects in our simplified modelling.

Finally, we turn to the dynamical results of van der Marel & van Dokkum (2007, hereafter MD07), who compiled $\Upsilon_{\rm dyn}$ for 60 local galaxies from the literature (van der Marel 1991; Magorrian et al. 1998; Kronawitter et al. 2000; Gebhardt et al. 2003; C+06). The original works made use of various types and quality of data and dynamical models, but should in general be superior to ours. The $\Upsilon_{\rm dyn}$ values are combined after homogenizing the distances and cosmology, and converting to the *B* band. As shown in Fig. B1 (right-hand panel), there is good agreement in general, but again a tendency for our results to overestimate the masses by ∼20 per cent, which appears to be an effect of the fainter, flatter galaxies. Note that our extrapolated σ_e shows no systematic offset from MD07. In order to potentially correct for a systematic error in our dynamical modelling, we adopt a heuristic correction of 66 and 90 per cent for faint and bright galaxies separately.

APPENDIX C: SYSTEMATIC UNCERTAINTIES FOR DARK MATTER FRACTION

We finally consider how various systematic uncertainties could impact the $f_{\rm DM}$ determinations. We first consider the stellar population models. As detailed in Appendix A, the model prescription that is used can have a notable effect on the $\Upsilon_\star$ trends. We show in Fig. C1 (upper-left panel) the differences engendered in $f_{\rm DM}$ by adopting different models. Among the most plausible models, the results are roughly consistent, but the trend of $f_{\rm DM}$ with luminosity tends to flatten or steepen with the use of M05 or BdJ01, respectively, rather than BC03.

We next consider uncertainties in the dynamical models, starting with the assumed mass profile. As shown in Fig. C1 (upper-right panel), the bracketing models of SIS and constant *M*/*L* produce similar results for $f_{\rm DM}$. Testing the possibility that our $n = 4$ Sérsic index for the bright Es is inaccurate, we alternatively take the higher $n-M_{\rm B}$ relation from Caon et al. (1993) as reported in PS97, and find that in a constant-*M*/*L* case, $\Upsilon_{\rm dyn}$ for the brighter galaxies decreases and the overall $f_{\rm DM}$ trend is constant with luminosity (Fig. C1, bottom-left panel). However, a SIS profile is probably a better match for these galaxies, and in this case, changing n would not affect the results. Finally, we try to calibrate out the inaccuracies in our simplified Jeans modelling, based on the MD07 results, and find that the $\Upsilon_{\rm dyn}$ values for the fainter galaxies might actually be lower, and the $f_{\rm DM}$ slope with luminosity therefore steeper (Fig. C1, bottom-right panel).

To quantify the effect of ellipticity (ϵ) on our estimates, we have also selected E galaxies with $\epsilon < 0.3$ (as derived by RC3). For these systems, the results are still consistent with an increasing (flat) trend of $f_{\rm DM}$ with luminosity for bright (faint) galaxies.

In summary, there are several potential competing systematic effects, and it is not clear which one might win out in biassing the $f_{\rm DM}$ slope. Given this uncertainty, we carry out a different, critical test of confidence in our results. Finding results in the literature for the mass content of galaxies in our sample *at large radii*, we construct the *M*/*L*-gradient parameter $\nabla_\ell\Upsilon$ introduced by N+05. This simple but powerful metric is calculated from dynamical measurements of *M*/*L* at inner and outer radii by the following formula:

$$\nabla_\ell\Upsilon = \frac{R_{\rm eff}}{R_{\rm out} - R_{\rm in}}\left(\frac{\Upsilon_{\rm out}}{\Upsilon_{\rm in}} - 1\right). \quad \text{(C1)}$$

Given the longer lever arm, $\nabla_\ell\Upsilon$ when available tells us with greater security whether or not an object is rich or poor in DM.[20] We compare $f_{\rm DM}$ and $\nabla_\ell\Upsilon$ in Fig. C2, and confirm that high-$f_{\rm DM}$ objects from this paper generally have high halo DM content in the literature while low $f_{\rm DM}$ have small $\nabla_\ell\Upsilon$ consistent with a lower global DM content.

[20] No attempt is made here to decompose the *M*/*L* measurements into stars and DM, i.e. to determine $f_{\rm DM}$. Instead, the broad premise is that $\Upsilon_{\rm dyn}$ increases more rapidly with radius in galaxies with higher $f_{\rm DM}$.

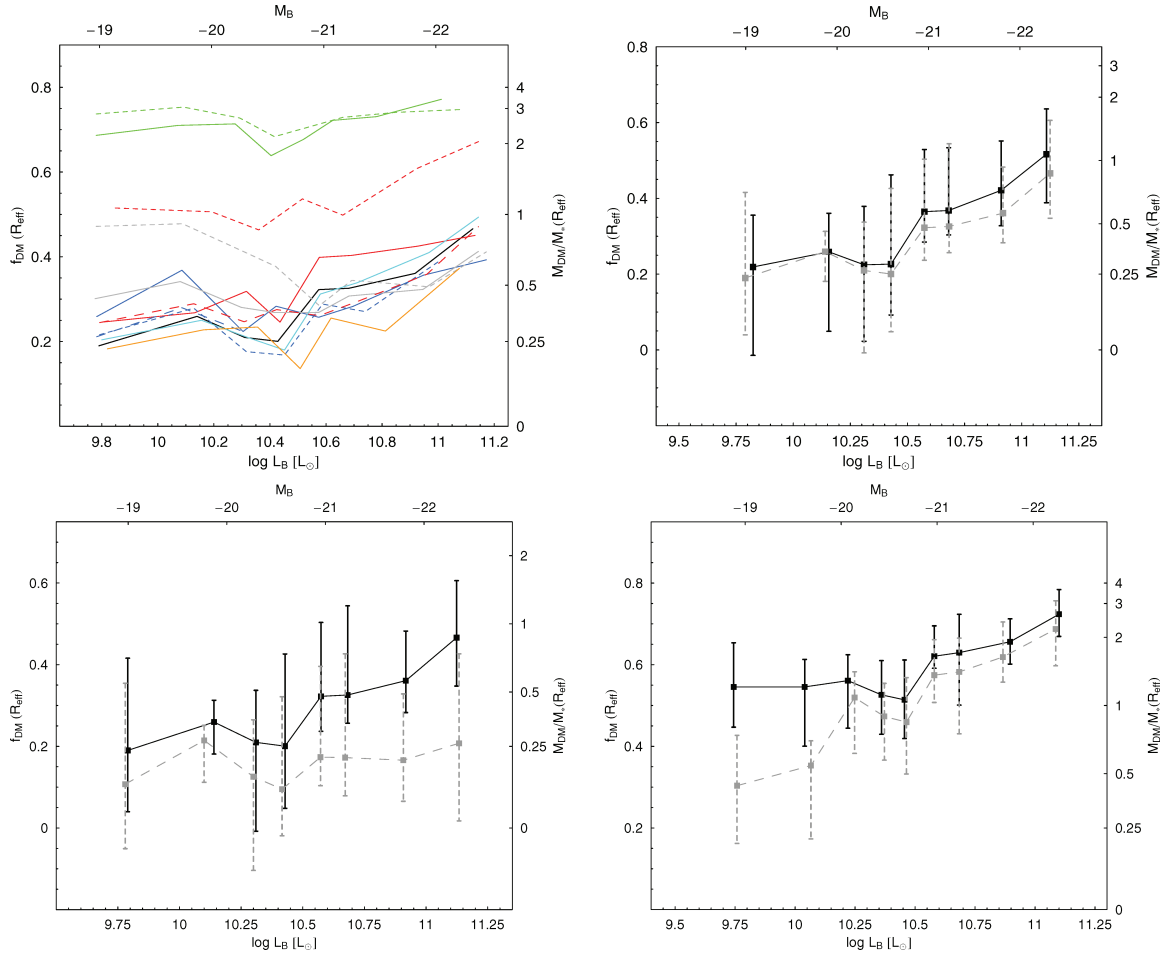

Figure C1. Effects of systematic modelling uncertainties on DM fractions, for the overall EG sample. Unless otherwise stated, the mass model is constant *M*/*L*, and the IMF is Salpeter. Top-left panel: changing the stellar population basis model (see left-hand panel in Fig. A2 for line definitions). Top-right panel: changing the dynamical mass model from SIS (black) to constant *M*/*L* (grey). Bottom-left panel: changing the Sérsic index *n* in the dynamical modelling [black: PS97 values; grey: Caon et al. (1993) values]. Bottom-right panel: calibrating the dynamical models using MD07 (black: original; grey: recalibrated). Here, a Chabrier IMF is used to avoid negative $f_{\rm DM}$ values.

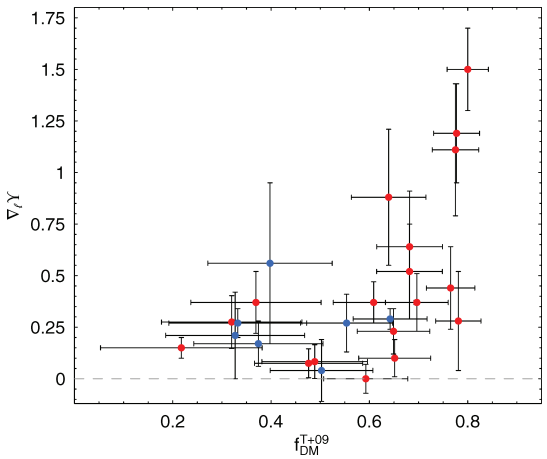

Figure C2. *M*/*L*-gradient parameter based on extended dynamics, compared to central DM fraction (default SIS model with Chabrier IMF). Red and blue dots are E and S0 galaxies. Most of the data are taken from N+05, with several updates and additions from more recent literature (Teodorescu et al. 2005; Schuberth et al. 2006; Douglas et al. 2007; Weijmans et al. 2008; Napolitano et al. 2009a; Kumar et al., in preparation; Romanowsky et al. 2008).

This paper has been typeset from a TEX/LATEX file prepared by the author.